Ore Geology Reviews 73 (2016) 522–539

Contents lists available at ScienceDirect

Ore Geology Reviews

journal homepage: www.elsevier.com/locate/oregeorev

A geological assessment of airborne electromagnetics for mineral exploration through deeply weathered profiles in the southeast Yilgarn Cratonic margin, Western Australia

I. González-Álvarez *, A.-Y. Ley-Cooper, W. Salama

CSIRO, Mineral Resources, Discovery Program, Kensington 6151, Australia

ARTICLE INFO

Article history:
Received 24 April 2015
Received in revised form 10 October 2015
Accepted 23 October 2015
Available online 29 October 2015

Keywords:
Regolith-dominated terrains
Mineral exploration through cover
Albany–Fraser Orogen
Yilgarn Craton margin
Airborne electromagnetics
Deep weathering
Ancient landscapes

ABSTRACT

Mineral exploration in regolith-dominated environments is challenging, requiring the development of new technical tools and approaches. When airborne electromagnetics (AEM) is combined with information on stratigraphy, mineralogy, geochemistry, drilling and landscape observations in a geological context, it becomes a powerful approach to describe the architecture of the regolith cover. This has significant implications for mineral exploration in any regolith-dominated terrain (RDT). This research presents two case studies of AEM data, integrated in a geological context for mineral exploration in the Yilgarn craton margin/Albany–Fraser Orogen (AFO). In one of the study sites presented (study site 1: Neale tenement), the availability of AEM data allowed for lateral and vertical extrapolation of the information contained in datasets at specific locations, thereby creating a 2D architectural model for the regolith cover. In addition, it was determined: (1) the total thickness of the regolith cover and its variability (between 2 m and ~65 m); (2) that low conductivity transported overburden and silcrete units, with a total thickness between ~5 and 45 m, is widely distributed, capping the upper saprolite; and (3) that the silcrete unit varies laterally from being completely cemented to permeable, and that these permeable areas ("windows") coincide vertically with mineralogical/textural/moisture/salt content changes in the underlying saprolite, resulting in increased conductivity. This has been interpreted as resulting from more intense vertical weathering, and consequently a higher vertical geochemical dispersion of the basement signature towards surface. AEM has been used to assist in identifying and describing the lateral continuity of these "windows" in areas with no direct field observations. Surface geochemical sampling above these permeable areas may deliver more reliable geochemical basement signatures.

In the second study site (Silver Lake tenement) the AEM data was strongly influenced by the high conductivity of the hypersaline groundwater. This had a significant effect on the AEM response, resulting in reduced depth penetration and reduced resolution of subtle conductivity contrasts between cover units. Despite this, the AEM data set, combined with geological observations in the area, was able to map the presence and extent of a buried palaeochannel network, the most significant architectural sedimentary feature in the cover. This interpretation allowed for a more efficient drilling campaign to be designed to sample the fresh basement rock suites in the area, by avoiding drilling into palaeochannels.

Integrated and constrained by the geological context, the application of AEM conductivity models by geologists is envisioned as one of the most promising tools within the exploration geologist toolbox to understand the architecture of the cover.

1. Introduction

Regolith-dominated terrains (RDT) are widely recognized as problematic environments for mineral exploration due to their lack of outcrop and deep weathering complexity (e.g., Smith, 1983; Butt, 1985; Anand, 2000; Butt et al., 2000; Vearncombe et al., 2000; Anand and Butt, 2010; Butt, 2016–in this issue; Porto, 2016–in this issue; González-Álvarez et al., in this issue-a; Xueqiu et al., 2016–in this issue). Basement geochemical signatures are masked within the cover due to the geochemical and architectural intricacy of the regolith (e.g., Robertson, 1996; De Broekert and Sandiford, 2005; Anand et al., 2014; Butt, 2016–in this issue; Porto, 2016–in this issue; Xueqiu et al., 2016–in this issue). However, geochemical dispersion processes throughout the regolith units may be locally efficient, producing metal anomalies corresponding to an ore footprint. These geochemical halos may be concentrated in a specific regolith unit, such as laterite or calcrete, and can reach the surface or form supergene ore deposits (e.g., Smith et al., 1987, 1989; Butt et al., 2000; Anand and Butt, 2010; Lintern, 2015). In mineral exploration, linking basement geochemical

* Corresponding author.
E-mail address: Ignacio.gonzalez-alvarez@csiro.au (I. González-Álvarez).

http://dx.doi.org/10.1016/j.oregeorev.2015.10.029
0169-1368/

features with surficial geochemical signatures is critical. To this end, the understanding of the cover architecture and its evolution is essential.

Climatic episodes of intense weathering under humid conditions, coupled with tectonic stability, may lead to large areas of deeply weathered landscapes: up to hundreds of metres in thickness, and therefore limited basement outcrop (e.g., Australia, Brazil, southeast India, southeast China). The chemically altered in situ rock may be covered by transported sediments, which all may be intensely weathered to the extent that the landscape becomes mainly flat and highly complex due to weathering overprinting (e.g., Anand and Butt, 2010).

Geophysical tools and approaches are being developed to assist mineral exploration in a RDT, such as remote sensing, radiometrics and radar, which feature only shallow penetration (<1 μm, <1 m and 1–20 m, respectively). However, technologies such as airborne electromagnetics (AEM) have potential ground penetration of up to >400 m and have been successfully applied in mapping groundwater and fluvial drainage systems (e.g., Reid et al., 2007; Munday et al., 2007), as well as in interpreting the diverse electrical conductivity variability within diverse regolith environments (e.g., Worrall et al., 1999; Munday et al., 2001; Ley-Cooper and González-Álvarez, 2014).

AEM has the potential to develop 3D stratigraphic correlations for the cover, based on the conductivity contrast between transported cover, in situ regolith and fresh basement rocks. This may improve interpretations of landscape evolution in a RDT. AEM can 'map' the surface of the weathering front (Anand and Butt, 2010 and references therein), and define differences in regolith stratigraphy based on properties of the features present that influence conductivity: clay mineralogy, porosity, permeability, and water content and chemistry (e.g., Reid et al., 2007; Ley-Cooper et al., 2008; Munday, 2009).

The southeast of Western Australia is an example of a RDT. It is largely overlain by a thick regolith cover, which extends from the Yilgarn Craton to the coastline, comprising the Albany–Fraser Orogen to the south and the Eucla Basin to the southeast (Fig. 1A and B; González-Álvarez et al., 2016–in this issue). This region contains limited outcrop, and is characterized by deeply weathered cover that evolved mainly during the Cainozoic (Pillans, 2005 and references therein).

This study advocates, from a geologist's point of view, how AEM data can be applied far beyond describing the electrical conductivity of the subsurface and detecting conductors at depth as potential targets for mineral exploration. When AEM is fully integrated in its geological context (geomorphology, stratigraphy, mineralogy, geochemistry, drilling, etc), it becomes a powerful tool to enhance the description of the architecture of the cover. This is exemplified in this research through two case studies of AEM applied to mineral exploration in a RDT in the southeast Yilgarn cratonic margin/Albany–Fraser Orogen.

2. Geological setting

The AFO is a Proterozoic orogenic belt adjacent to the southern and southeastern margins of the Archaean Yilgarn Craton in Western Australia (Fig. 1C). Study site 1 (Neale tenement) is located in the AFO, 60 km northeast of the Tropicana-Havana Au system (Fig. 1A; ~6800000 E, 700000 N UTM, Zone 51). According to Spaggiari et al. (2015) the AFO is the result of the preservation of the southeast Yilgarn Archaean Craton margin that records Proterozoic tectonic changes. These changes were dominated by extensional processes that generated a wide variety of basins and concomitant magmatic activity.

The AFO lithologies are characterized by the Archaean Northern Foreland (metagranitic and metamafic rock suites); the Archaean-Proterozoic Tropicana Zone (with abundant granites); and the Palaeoproterozoic Birunup and Nornalup zones (~1.8–1.6 Ga orthogneiss, metagabbroic and hybrid rocks); the Mesoproterozoic Fraser Zone, and Recherche and Esperance supersuites (~1.3–1.1 Ga metagabbroic and granites rock suites, respectively; Spaggiari et al., 2015 and references therein; Fig. 1C). Eastwards the Phanerozoic sedimentary and volcanic units of the Eucla Basin largely cover the AFO.

The Neale study site is located above the Tropicana Zone, with local outcropping of the Carboniferous-Permian Paterson Formation, Archaean gneiss, the McKay Creek Metasyenogranites and to the east the Palaeoproterozoic Black Dragon gneiss (metagranodiorite and granodiorite; Kirkland et al., 2015; Fig. 1C). The main structural trend in this area is northeast/southwest, which is punctuated by the geometry of the main lithological units (Fig. 1C), together with structural shear zones and magnetic trends (Kirkland et al., 2015).

Study site 2 (Silver Lake tenement; Integra Mining Ltd./Silver Lake Resources) is located in the southeast of the Yilgarn Craton, which is a granitic-greenstone belt characterized by metamorphosed sedimentary–volcanoclastic sequences that reside among large granite-dominated areas. The Yilgarn is dominated by undivided granites to the east (Fig. 1C) and greenstone belt sequences to the southwest (Fig. 1C), together with the Widgiemooltha Dyke suite in the south and north. The most significant geological trend is displayed by elongated domains stretched in the northwest/southeast and southwest-northeast directions (Fig. 1C).

The Silver Lake site is located in the Kurnalpi Terrane (Fig. 1C), which is one of the six terranes of the Yilgarn Craton (Cassidy et al., 2006). The Kurnalpi Terrane is bounded by an interlinked fault system and jointly comprises the Eastern Goldfields Superterrane. It has an estimated age of crustal formation ~3.1–2.8 Ga, with depositional greenstone belts ~2.94–2.66 Ga, coupled with a wide diversity of ages for granite and gneiss emplacement that vary from 2.81–2.62 Ga. The main deformational and metamorphic events identified spanned from 2.67 to 2.63 Ga (Cassidy et al., 2006).

Two relatively recent mineral exploration discoveries have generated interest in the southeast Yilgarn Craton margin-AFO region (Fig. 1): (1) the ~2.52 Ga Tropicana-Havana gold system with 6.41 Moz Au, discovered in 2005 (Doyle et al., 2015); and (2) the Nova-Bollinger Ni–Cu deposit discovered in 2012 in the Fraser Range (ore reserve estimate 13.1 Mt. @ 2.1% Ni, 0.9% Cu and 0.07% Co; IGO website, October 2015).

3. Regolith setting

The weathering framework of the region can be summarized in stages that were initially dominated by fluvial sedimentary systems during the Palaeozoic and Mesozoic. From the Permian to Late Cretaceous humid sub-tropical conditions promoted intense chemical weathering, which shifted in the Late Tertiary to semi-arid conditions (Anand and Butt, 2010 and references therein).

The Neale area is situated on a drainage divide between 300 and 400 m elevation, with the main drainage directed towards the Eucla Basin in the southeast (Fig. 1A and B). Native grasslands dominate this area, with extensive aeolian sand dunes present, characterized by 3300 mm annual potential evaporation and average rainfalls of 200 mm (Fig. 1B and D; Anand and Butt, 2010). The dominance of evaporation has resulted in groundwater salinities of 1000–3000 mg/L TDS (Total Dissolved Salt; Fig. 1D; Commander, 1989). The pH of the groundwater is expected to be low since basement is dominated by granitic gneisses (Gray, 2001). Groundwater salinity, acidity and chemical ligands are key factors that control trace element mobility.

The Silver Lake study site is mainly low relief in the south, with gently undulating and sporadic dissected scarps of granites and greenstone ridges, and primarily high relief in the north. The Digital Elevation Model (DEM) indicates that most of the tenement elevation lies between 150 and 400 m (Fig. 1A). The area is associated with a large palaeodrainage system that drained to the east (Fig. 1D). Numerous saline lakes characterize the drainage system in the central and southern areas (Fig. 1A and D). The vegetation cover is characterized by native grasslands and woodlands. These surficial features reside upon saprolite, as well as colluvial and alluvium sediments, with few outcroppings. The regolith is characterized by residual and calcrete duricrust outcroppings to the south (Fig. 1B).

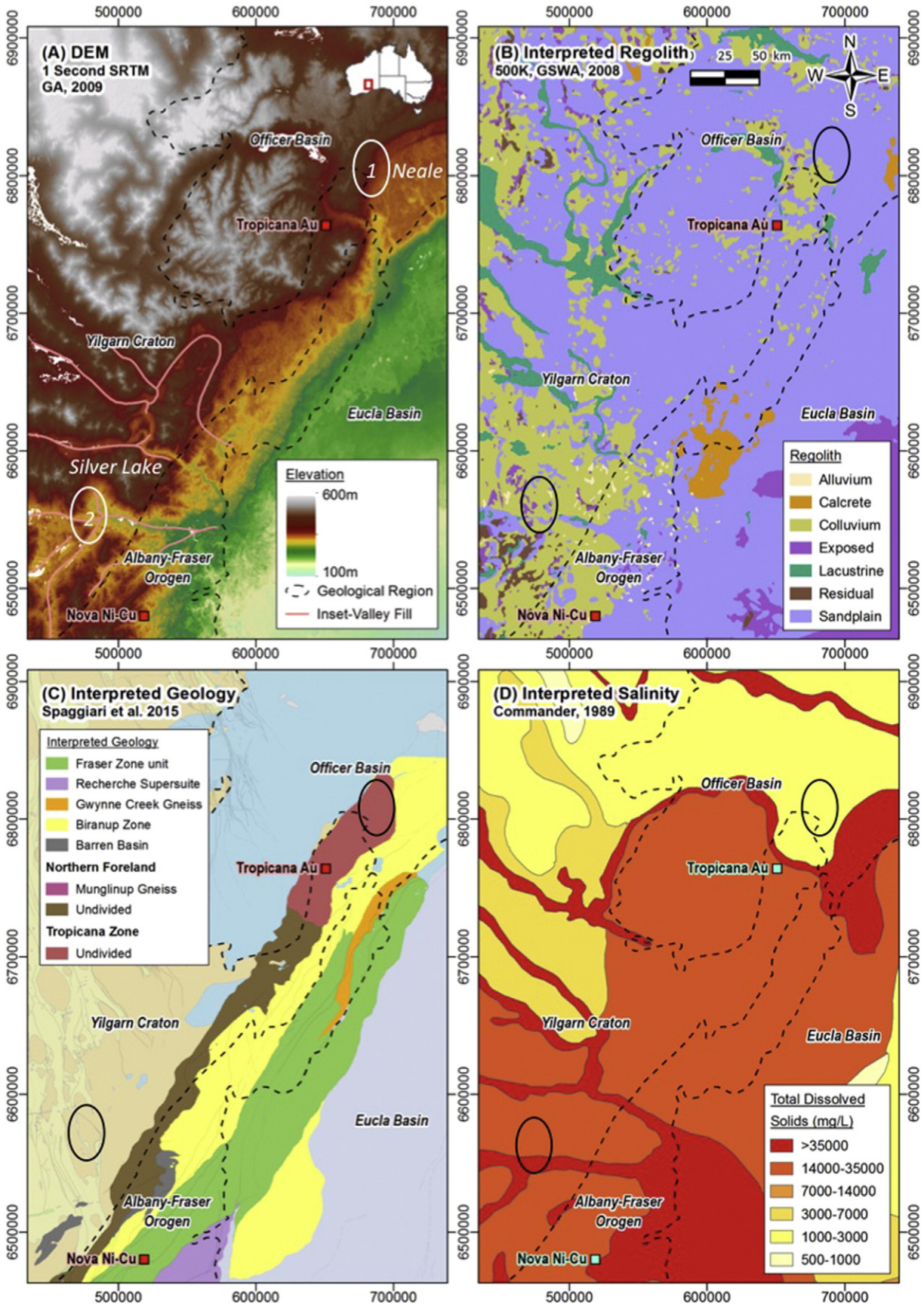

Fig. 1. Maps of the regional geological context of Neale and Silver Lake: (A) Digital Elevation Model (DEM) indicating the topography of both study sites; (B) regolith map, which indicates that Neale is dominated by sandplain facies deposits whereas Silver Lake is dominated by colluvium and residual regolith deposits; (C) interpreted basement geology, showing that both sites feature Archaean basement rock suites at depth (modified from Spaggiari et al., 2015); and (D) large scale salinity map, which indicates that Neale is located in an area of low salinity groundwater, whereas Silver lake lies above a palaeochannel containing hypersaline groundwater.

4. Methodology

For the Neale tenement, 32 reverse circulation (RC) and diamond drill (DD) cores were described from three reference profiles, which delineated the variability, thickness and characteristics of the regolith (Fig. 2). This was coupled with field observations to review the regolith sections described from the drilling of the different units of the transported cover, together with the in situ regolith. Stratigraphy of the Silver Lake cover was described using company data from drill holes and previous lithological information (Integra Mining Ltd./Silver Lake Resources).

For AEM data collection, a fixed-wing time domain EM survey of ~600 line km was carried out in both study sites (Neale and Silver Lake; Figs. 2 and 3). For Neale an AEM survey was designed for an

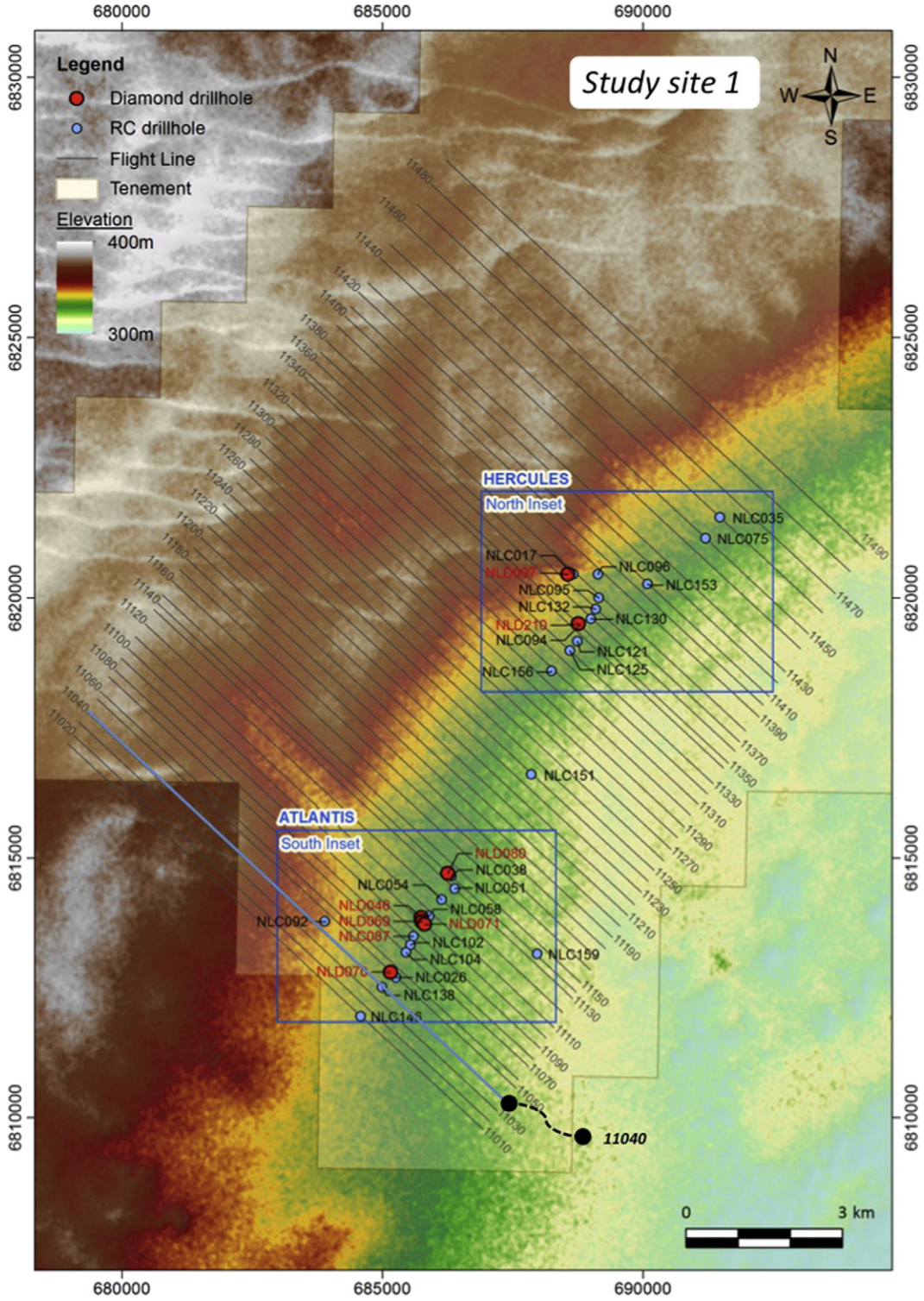

Fig. 2. Airborne electromagnetic (AEM) flight path array flown over the 32 RC and DD drilling holes, which were logged to determine regolith stratigraphy. Based upon the drill hole datasets (Beadell Resources Ltd.) the study area was divided into two Au prospects: Hercules and Atlantis (MGA51). Flight paths for AEM data collection were designed to pass directly above the drill holes to enable the cross-referencing of the conductivity responses in the regolith to direct stratigraphic observations. Line 11040 highlighted for reference in the methodology section.

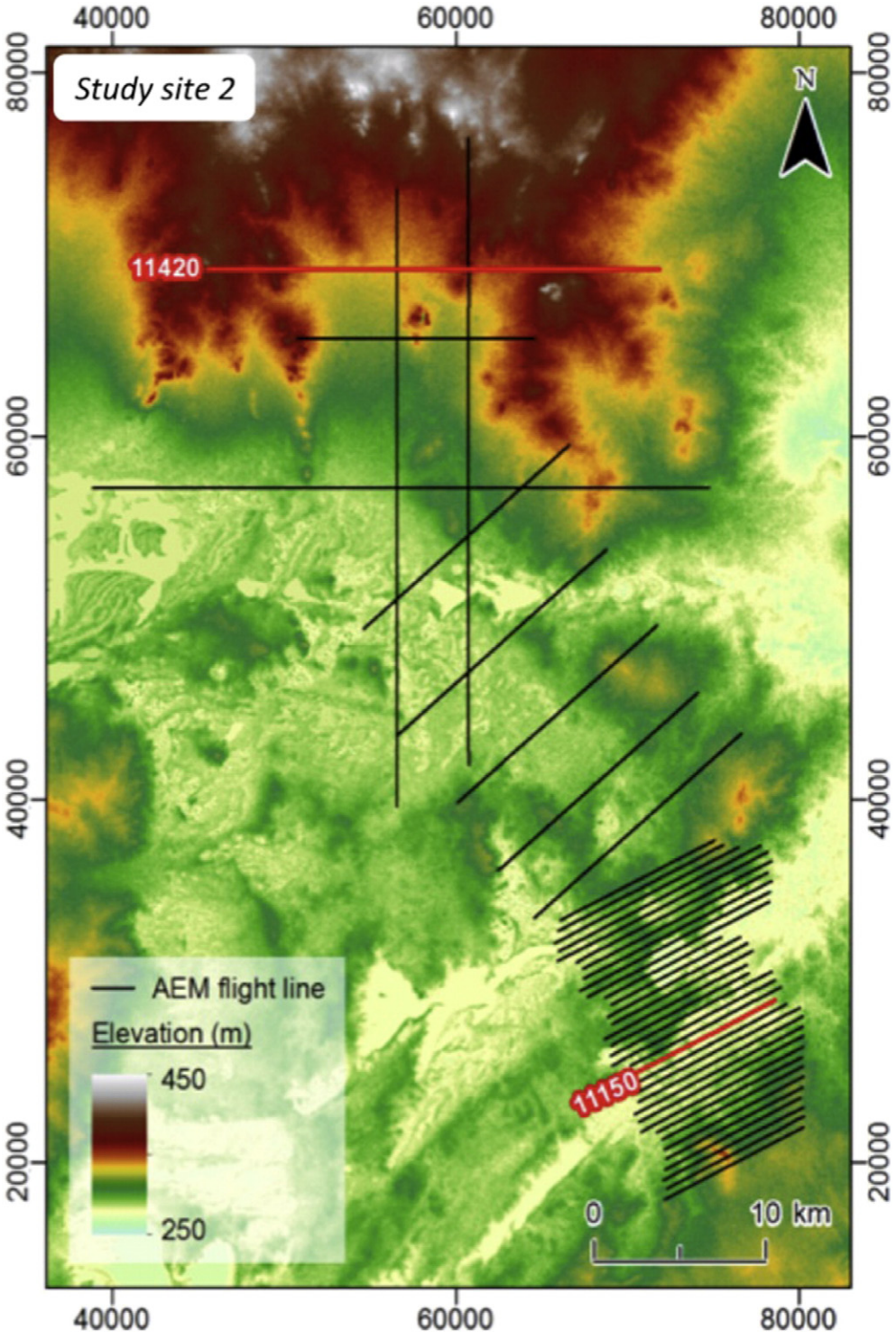

Fig. 3. AEM flight paths over the Silver Lake area with two paths highlighted in red, which exemplify paths flown for regional contextual interpretation (11420) and for detailed overburden interpretation (11150). The denser array of AEM flight paths in the southeast was designed to resolve the geometry of the palaeochannels intersected by numerous drill holes in this area.

area of ~120 km^2 with AEM lines planned to pass over available diamond and reverse circulation (RC) drill holes (Fig. 2), whereas for Silver Lake the total area covered was over 500 km^2 (Fig. 3). In Silver Lake, the northern part of the survey was flown to collect data on regional cover and basement structures, hence the broad line spacing between flight lines in that region (Fig. 3).

4.1. The Spectrem$_{2000}$ AEM system

AEM instrumentation has been developing since the 1950s. Spies et al. (1998 and references therein) presented a compedium of the literature, and Davies (2013) described how the technique has developed up to the present. The AEM instrument's transmitter induces a current

into the Earth by generating an electromagnetic field. The ground exposed to this primary field will in turn generate a secondary field response that is recorded at the instrument's receiver. From this the instrumentation is able to record the conductivity of the ground at depth. In areas with regolith cover this methodology is efficiently applied to delineate basement surfaces, since fresh basement rock suites generally present a significant change in conductivity relative to the weathered profiles above.

The AEM system employed in this study was a Spectrem$_{2000}$, which is a fixed-wing time-domain system that has been in use since 1989, mainly in Australia, Canada and Africa (Leggatt et al., 2000). This system was designed to map high-conductive bodies at depth. Its resolution is dependent on the specific electrical properties of the ground units, and the lateral and vertical extent of target bodies. Spectrem$_{2000}$ has been used to efficiently map and discriminate targeted geological units to depths of hundreds of metres such as in Canada (fresh rock outcrops, tillite and ice) and Australia (deeply weathered profiles with abundance of high salinity groundwater; Leggatt et al., 2000; Pare et al., 2012; Ley-Cooper and González-Álvarez, 2014).

This instrument employs a bipolar 100% duty cycle approximately square-wave current pulse (primary field), which operates at variable base frequencies of 25 Hz and higher. Further processing is needed in order to discriminate the primary field from the induced secondary field to improve accuracy. At each station the EM decay is processed as a step response, which is averaged and then sampled into 10 time windows. In this processing, the last window of the decay is subtracted from all of the earlier windows in an attempt to remove the transmitted primary pulse present in the recorded response. The underlying assumption is that during the last half of the decay, the secondary field is nearly zero and what remains is only the coupling coefficient of the primary field (Ley-Cooper and Munday, 2013).

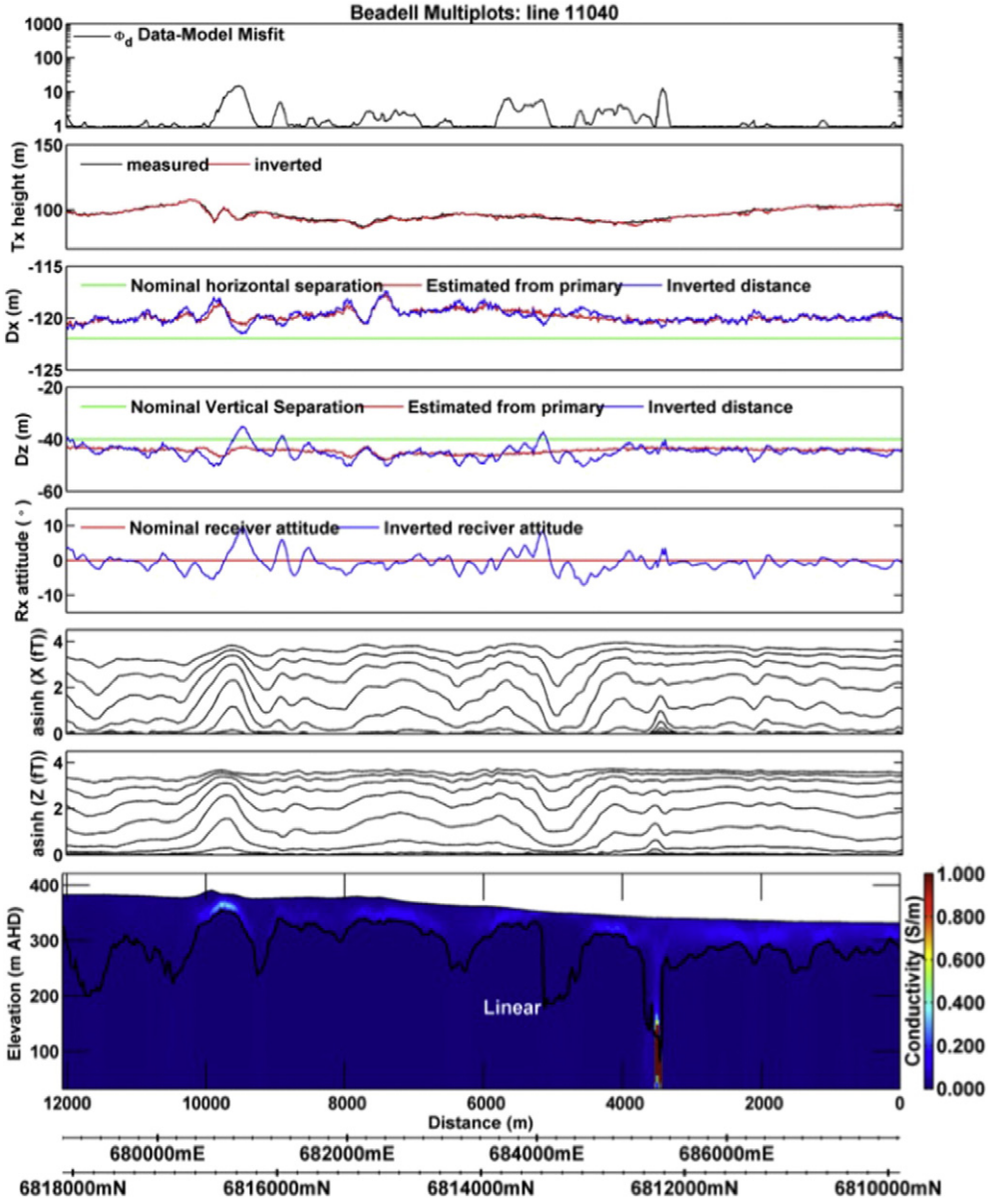

Fig. 4. Example of a multi-panel plot used for data analysis and derived inversions based on a target anomaly in the basement at Atlantis (line 11040; Fig. 2). The top panel is a profile of parameter ϕ_d, which we calculate and use as an indicator for assessing the level of fit between our measured data and our proposed models derived from inversion. Lower values of ϕ_d reflect a better agreement between models and measurements, with the optimum value being one. Other parameters plotted are the vertical and horizontal separations (Dz, Dx) of the transmitter–receiver, and asinh Z(fT) (inverse hyperbolic sine function, in femto teslas) and asinh X(fT), respectively. All panels are used to measure quality assurance and interpretation validity of the analysis of the AEM data presented in the lower conductivity-depth section.

4.2. Data assessment

The Spectrem$_{2000}$ dataset was inverted using Geoscience Australia's sample-by-sample Layered Earth Inversion Algorithm (GA-LEI; Fig. 4, line 11040 from Fig. 2), which is described in Brodie (2012), and Ley-Cooper and Brodie (2013).

As an AEM's secondary magnetic field migrates through the ground, resembling a "smoke ring", it becomes increasingly diffuse the deeper it penetrates. The vertical resolution of the AEM is dependent upon the conductivity of the subsurface and the contrast in conductivity between layer interfaces. Macnae et al. (1991) suggested a numerical calculation for vertical resolution of a towed bird system like Spectrem$_{2000}$. They estimated that the maximum vertical depth at which the signal-to noise-ratio could still resolve conductive structures was ~600 m. However, the vertical resolution was a fraction of the noise relative to the transmitter–receiver separation (Tx–Rx). This established that conductive units ~5–10 m thick, only a fraction of the transmitter–receiver separation, could be defined in a given survey as long as the signal-to-noise ratio remained between 0.2–0.5%, depending upon the geological context. For a Tx–Rx nominal distance of 120 m, Macnae et al. (1991) reported a theoretical vertical resolution of 6 m thickness.

A further description of the system's specifications and other instrument particulars can be found in Leggatt et al. (2000). Ley-Cooper and Brodie (2013) discussed how the instrument's Tx–Rx coil position fluctuations will cause the primary and secondary fields to fluctuate at the receiver. Through modelling it was determined that an accurate knowledge of the position and orientation of the receiver bird was important for resolving near surface variation in conductivity, with implications for mapping regolith variability.

For this work we used a 30 layer model, which it was defined starting at 4 m thickness and increasing in a logarithmic scale to reach an accumulative total depth of 600 m. We determined a multiplicative noise value of 0.3 %, for high altitude flights, and employed this measure for modelling using the GA-LEI inversion. The GA-LEI algorithm inverts the total field data (primary plus secondary) and solves for parameters that describe the relative geometry between the transmitter-receiver, such as the horizontal and vertical offsets, and the instrument's rotation. Tx–Rx separations were considered and modelled to vary with 5% of their nominal values of 120 m horizontally and 45 m vertically for this survey.

Fitterman and Stewart (1986) presented the feasibility of using time domain electromagnetic methods (TDEM) to solve groundwater-related issues. Specifically, they articulated a methodology to detect saline and brackish water interfaces in freshwater aquifers if there is enough conductivity contrast. They reported that the methodology was efficient in mapping conductive targets, such as salt-water layers in the ground, as well as alluvial fill and gravel zones over bedrock, even when covered by a thick conductive clay layer. They show electromagnetic methods can be used to map basinal and palaeochannel brines in areas of contrasting groundwater salinities. However, in many areas in Australia where saline groundwater conditions prevail, AEM penetration depth is limited, along with its ability to discriminate between individual regolith units and boundaries, since the signature of the more conductive groundwater solution overprints the more subtle conductive contrasts of other units. Figure 5 shows an example of the spatial distribution in the Neale site of conductance.

Figure 5 shows an example of the spatial distribution in the Neale site of conductance from different materials at depths ranging from 18 to 25 m. Joint analysis of inverted cross-sections along the flight paths and conductivity maps at different depths enabled delineation of zones that correspond to transported and weathered sequences of sediment and altered rock, and also the determination of their thicknesses and lateral extent. Maps were produced for inverted depth conductivity slices to calculate maximum regolith thickness and describe the buried surface of fresh basement rock suites. Maps at depths of ~300 m and below were deemed beyond the system's depth penetration (Christiansen and Auken, 2010) under these particular conditions, which were calculated based on the final conductivity model.

An AEM fixed wing system flying at 70 m from the ground, samples an area of ~100 s metres laterally. Vertically its' resolution will depend upon the conductivity contrast between the layers, the noise levels and discretization of the layered-earth model employed. We grouped the regolith materials from drill holes in packets that are >4 m, to try and ensure they are resolvable by the AEM. The thickness of the regolith cover from the inverted AEM models, is then determined by 1) the morphology of the stitched conductive models, and 2) by using a threshold cut-off value of conductivity.

5. Results

The logging of 32 RC-DD drilling holes in the Neale tenement has recorded a variable transported cover of regolith between 2 and 25 m in thickness. This regolith stratigraphic package is characterized by Fe-stained ferruginous, polymictic sand and gravels, which are clast-supported with variable sorting (Fig. 6). An idealized section indicating the types and representative thicknesses of stratigraphic units described at the Neale site is given in Fig. 6.

The in situ regolith is divided into three units: (1) a laterally continuous silcrete unit (4–20 m thickness) with variations in the extent of silica cementation; (2) a sandy-kaolinitic upper saprolite; and (3) a lower saprolite mainly expressed as ferruginous parental rock (granites, gneisses, schists and mafic rock suites). The upper and lower saprolite packages vary from 18 to 50 m in thickness. The saprolites and silcrete unit have a combined thickness ranging from 22 to 70 m (Figs. 6 and 7). Silver Lake AEM data were processed to derive an estimate of regolith thickness variability from the inverted conductivity depth models, the results of which are displayed in Fig. 8.

These spatial plots indicate that the variability of the regolith thicknesses are not directly related to topographically high and low areas. This indicates that a range of factors may be contributing to the development of a complex weathering front. In the Neale tenement, the thickest regolith packages are in the north of the flown area, which coincides with the highest elevation, whereas the Silver Lake study site displays significant variability of regolith thickness within the main low area structure defined in Fig. 8 (varying from 2 m to ~110 m). This underscores the importance of the use of AEM to help understand the influence of weathering fronts by the complexities of the basement and how they evolve at depth (e.g., structure, alteration, metamorphism, rock type, etc).

In the Neale tenement, field observations were compared with AEM data, which indicated regolith thicknesses ranges from ~5 m–~70 m (Fig. 7). The consistent agreement between drilling information and interpreted AEM data strongly supports the effectiveness of AEM to infer total regolith thickness in the area. The difference between maximum drilling depth of ~70 m and a AEM-derived depth of ~65 m is within the range of AEM interpretation and logging uncertainties. In the Silver Lake tenement, the cover thickness is interpreted to have a wide range of values, reaching values from ~5–~110 m (Fig. 8).

5.1. AEM conductivity-depth sections

Based on the inverted AEM and the logging of the regolith profile in the DD-RC drill holes available, three conductivity-depth sections were selected: Profiles 1, 2 and 3, displayed in Fig. 9 below. These profiles contain drilling information used for the interpretation of the regolith architecture at the Neale study site. AEM interpreted Profiles 1, 2 and 3 are presented in the Discussion Section, as well as interpreted key profiles for the Silver Lake tenement. This was used to describe the geometry of the stratigraphic units both laterally and vertically, and therefore to infer stratigraphic features between drill holes.

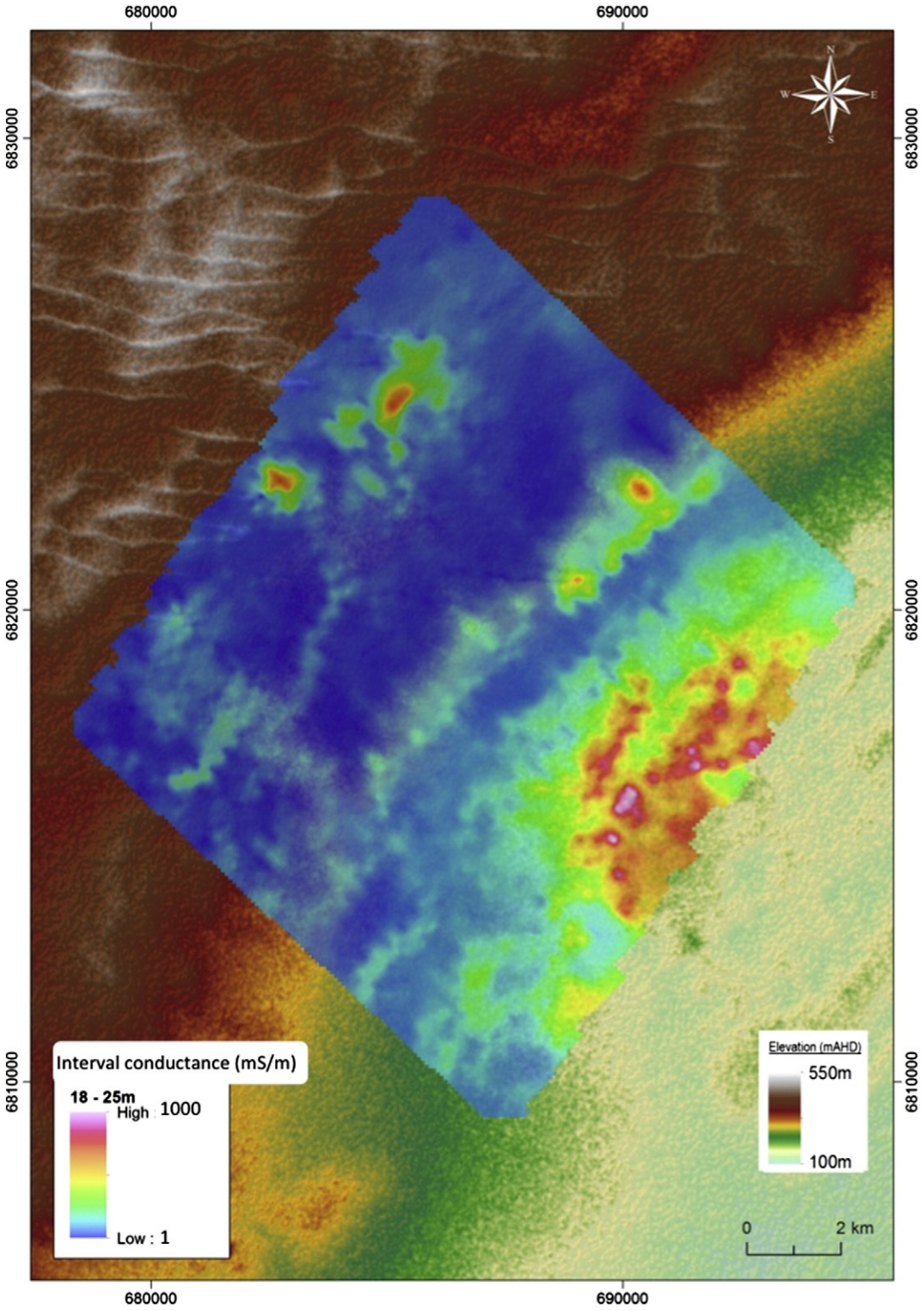

Fig. 5. Example of an average conductance depth slice from the GA-LEI inversion of the AEM data at Neale. Depth ranges from 18 m to 25 m. The conductivity map is displayed for the DEM of the area. This data indicates a more highly conductive area to the southeast, which corresponds to thickening overburden towards the Eucla basin.

6. Discussion

6.1. Drilling and AEM integration in the geological context: regolith architecture

AEM has been suggested as a tool to map regolith-dominated regions based on its ability to differentiate conductivity contrasts in regolith (Palacky et al., 1981). Materials such as sulphides, graphite, saprolite, clay-rich sediments and saline groundwater are good conductors. In very resistive lithologies, a small response from the ground is measured, but when the EM system is flown over a conductive geological unit, a higher amplitude can be measured. Therefore, if conductivity contrasts are present, they can be interpreted in the geological context of the cover (Ley Cooper, 2013; Fig. 10, modified after Palacky, 1987).

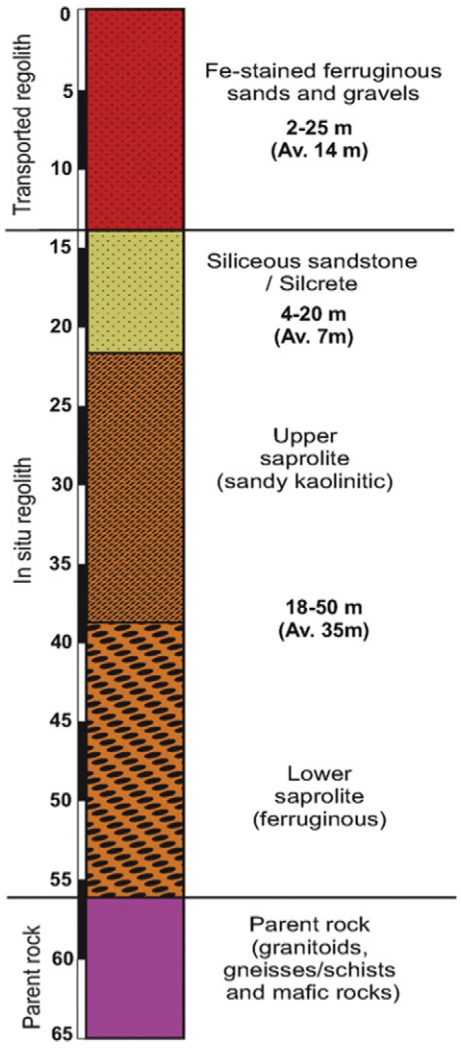

Fig. 6. Ideal stratigraphic sequence of the regolith profile at Neale. This profile displays ~10–45 m of low conductivity units located at the top of the regolith sequence, underlain by ~20–50 m of saprolite comprising quartz and different clay mineralogy. Further data on the mineralogy and geochemistry of this regolith environment can be found in Salama et al. (2016–in this issue).

AEM methodology is a tool to define the architecture of the cover and therefore to enhance the understanding of landscape evolution in RTDs (e.g., Worrall et al., 1999; Munday et al., 2001; Worrall et al., 2001).

6.2. Insights on mineralogy, petrophysics and conductivity in the regolith

Regolith units are the result of in situ and/or transported material which has been affected by weathering processes. This results in the hydrolysis of ferromagnesian minerals and feldspars, which are the most abundant minerals in the crust (Nesbitt and Young, 1982). Weathering processes release Na, Mg and Ca from minerals and transform them mainly into clay minerals. This results in the high abundance of clays in most of the regolith throughout Australia. Intense weathering conditions result in kaolinite-rich regolith units predominantly over felsic rock suites, and smectite-rich units over mafics and ultramafics rock suites. Physical, specifically electrical, properties of the regolith are strongly affected by its clay mineral content (>40 mS/m; Rutherford et al., 2001).

Munday et al. (2001) reported that the electrical conductivity of regolith units in the Yilgarn Craton depend mainly upon petrophysical properties such as porosity, texture, moisture, salt content and clay mineralogy (which determines the cation exchange capacity of the clay). Based upon laboratory studies, Emerson and Yang (1997) reported low conductivity responses for clean sands and pure kaolinite (3 mS/m, due to their low capacity for cation exchange). However, this conductivity was enhanced when kaolinite was mixed with sand- and silt-sized sediment (10 mS/m). Bentonites were reported to have high conductivities ranging from ~65 to ~120 mS/m (Emerson and Yang, 1997). Drill hole petrophysical data in the Eastern Goldfields region have suggested that an important control on regolith conductivity is moisture content and soluble salts (Munday et al., 2001). The precipitation of salts in the pore spaces or the presence of moisture within the regolith units has an important effect upon enhancing the electrical conductivity of the unit.

The contact between regolith and fresh basement rock is commonly transitional regarding its electrical conductivity properties, since it is the transition from unweathered bedrock to heavily weathered saprolite. The contrast in the electrical conductivity of this transitional layer and basement rocks is normally pronounced enough to define a transitional zone to separate both (Emerson et al., 2000).

6.3. Salinity and digital elevation complexities: palaeovalleys and palaeochannels

One of the most striking geomorphological features in the Yilgarn Craton margin/Albany–Fraser Orogen is the presence of an extensive palaeodrainage system (e.g., Clark, 2009). From the late Tertiary to the Quaternary, semiarid to arid climatic conditions were widespread in the Yilgarn. This resulted in the failure of major river systems, which converted into a sequence of lakes. At the same time, surface and groundwater became increasingly saline (De Broekert, 2002).

Palaeochannels in the Yilgarn Craton correspond to zones of unconsolidated sands that are saturated with saline brines (e.g., Smyth and Barrett, 1994; De Broekert, 2002 and references therein). The subsurface water flow becomes increasingly saline moving down slope, and these high salinity waters accumulate in the sedimentary package-filled channels. This produces a strong conductivity contrast between the saline saturated palaeochannel sedimentary sequences and the basement rock suites, and in some cases between Tertiary sands and saprolitic bedrock (Smyth and Barrett, 1994). Saline water is concentrated in the river sedimentary sequences where there is higher porosity and permeability, and therefore can be used as a tracer defining potential palaeochannels from groundwater salinity maps (Fig. 1D). This has a significant influence on the interpretation of AEM data in the Yilgarn Craton and on it's margins.

At Silver Lake, Commander (1989) recorded groundwater salinity values >35,000 mg/L TDS that were interpreted to be associated with the confluence of large palaeochannels (Fig. 1D). This hypersaline feature in Silver Lake has significant effects on the trace element mobility within the regolith and its expression at surface, since element dispersion is driven mainly by fluid conditions: salinity, acidity (pH) and oxidation-reduction potential (Eh) (e.g., Kyser et al., 2000; Kerrich et al., 2002). This contrasts with the Neale study site where water salinity values have been reported as <3000 mg/L TDS (Fig. 1D). Hence these study sites have a significantly different framework for their geochemical exploration protocols and anomaly interpretations, as well as for ground responses detected by AEM.

Figs. 7 and 8 display the interpreted total regolith thickness of the two study sites (Neale and Silver Lake, respectively) on the multi-resolution index of valley bottom flatness (MrVBF) map. This map is derived using the Gallant and Dowling (2003) algorithm that describes the landscape, enhancing bottom features of valleys. It discriminates between uplands (dark grey) and lowlands (white). Taking into consideration the geomorphological context, light grey colours may indicate the presence of deactivated landscape features such as palaeochannels, palaeodrainages and palaeovalleys, which may be expressed as relatively flat areas. Hence the MrVBF algorithm has the potential to map the main depositional areas and geomorphological domains. The relationship between MrVBF and thickness of the transported cover is especially of interest in areas geomorphologically dominated by fluvial

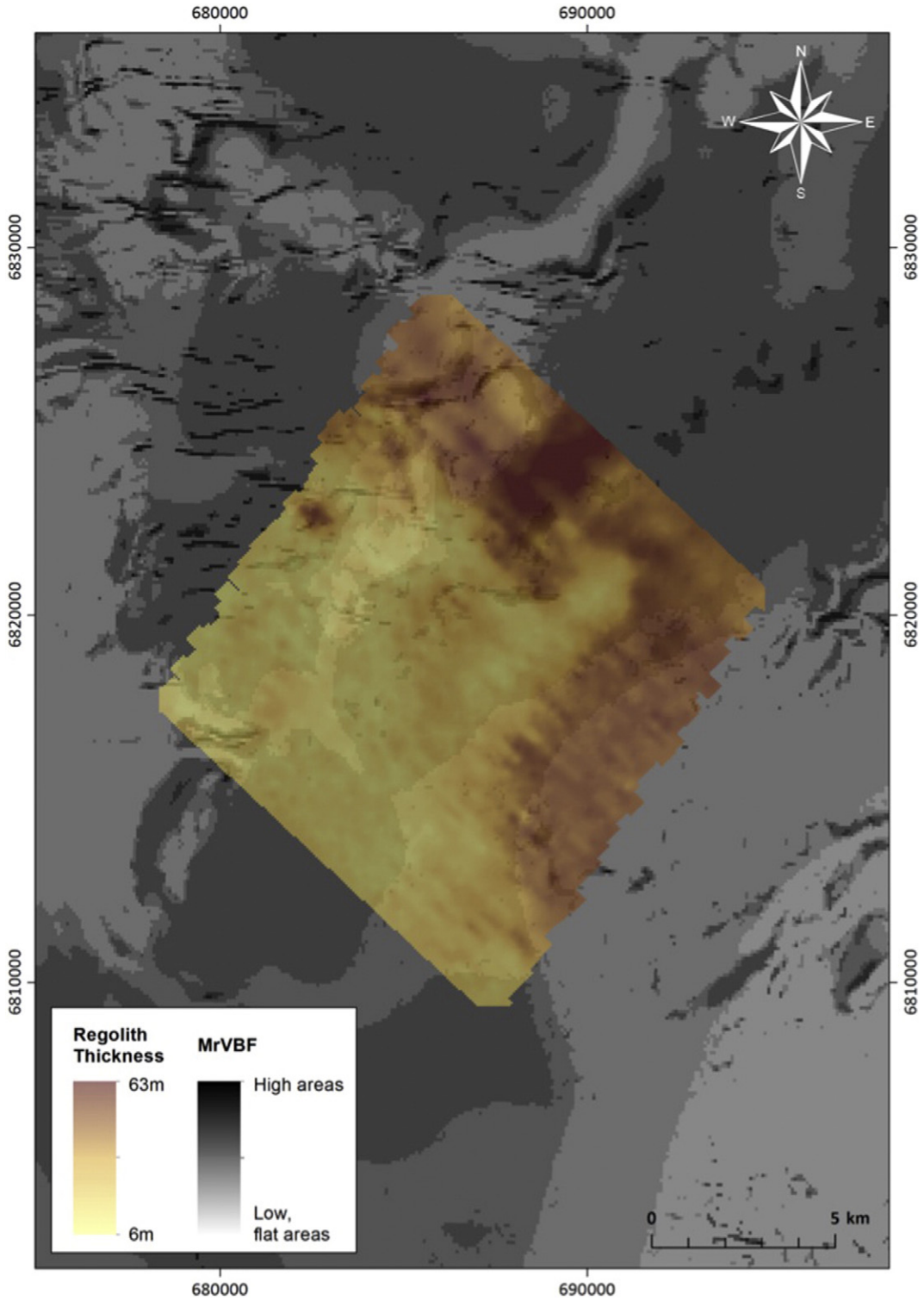

Fig. 7. AEM-interpreted regolith thickness of Neale combined with the MrVBF map. This image displays that regolith thickness does not directly correlate with the flatness of the surface, as the thickest regolith is located in the north in areas of high relief and slope. Neale area delineated on the MrVBF map, including the AEM flight paths marked in yellow. This figure reveals the Neale area covering a geomorphological irregular region, close to the flat-dominated Eucla basin overburden to the southeast.

sedimentary systems, since flatness of the landscape can be correlated with palaeochannel features.

Fig. 7 presents the thickest regolith in the Neale area: in the north-northeast and in the southeast of the surface surveyed. The southeast area can be linked with the thicker transported cover associated to the Eucla basin sediments. However, the north-northeast ~60 m regolith thickness corresponds to an area with an elevation of ~400 m high (DEM; Fig. 1A) and higher topographic variability. This exemplifies how the weathering front possesses a complex geometry. It is possible that weathering was constrained along narrow structures such as shear zones or faults, however, more information needs to be collected to substantiate this hypothesis.

Fig. 8 displays the same dataset combination as Fig. 7 for the Silver Lake area. In Fig. 8 several palaeo-geomorphological features can be

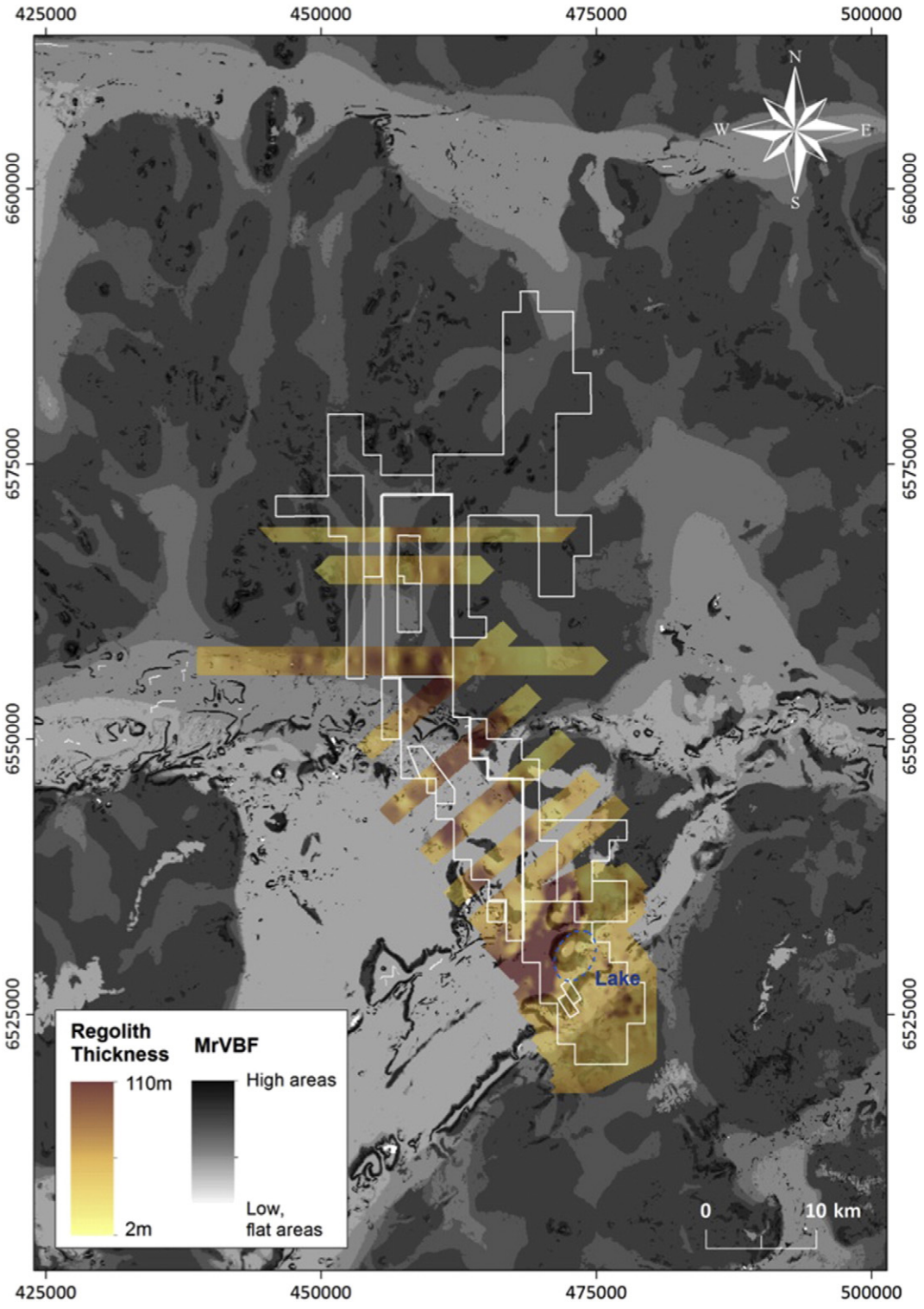

Fig. 8. AEM-interpreted regolith thickness iso-map of the Silver Lake study site over the MrVBF map. White polygons correspond to the Silver Lake Resources tenement boundaries. The thickest regolith (~100 m) is located to the southeast where the main palaeochannel structure exists. This figure indicates a regolith thickness trend from thinnest to the northwest to thickest to the southeast. MrVBF map of the Silver Lake area showing the surveyed AEM flight lines, with the interpreted palaeochannel axes in blue. This map reveals the palaeochannel join in the area, adding contextual geomorphological information. This area contains hypersaline groundwater (Commander, 1989), which was sampled in the same palaeochannel structure at boreholes ~30 km to the east of the study area. All sample analyses gave 30,000- >75,000 mg/L (TDS; Gray, personal communication, 2015).

identified: (1) a drainage system which describes how the contemporary landscape links saline lakes and to palaeodrainage channels (Fig. 1D) and (2) palaeovalleys. The maximum regolith thickness interpreted from the AEM data coincides with flat areas that are related to the palaeodrainage system in the area. These features were developed when rivers in the Yilgarn Craton drained to the east (into the Eucla basin) during the Eocene, and the shoreline was close to Kalgorlie (De Broekert, 2002). The thickest regolith package is in an area where the main palaeochannels joined (Figs. 1D and 8; De Broekert, 2002). These large palaeochannel infills are characterized by

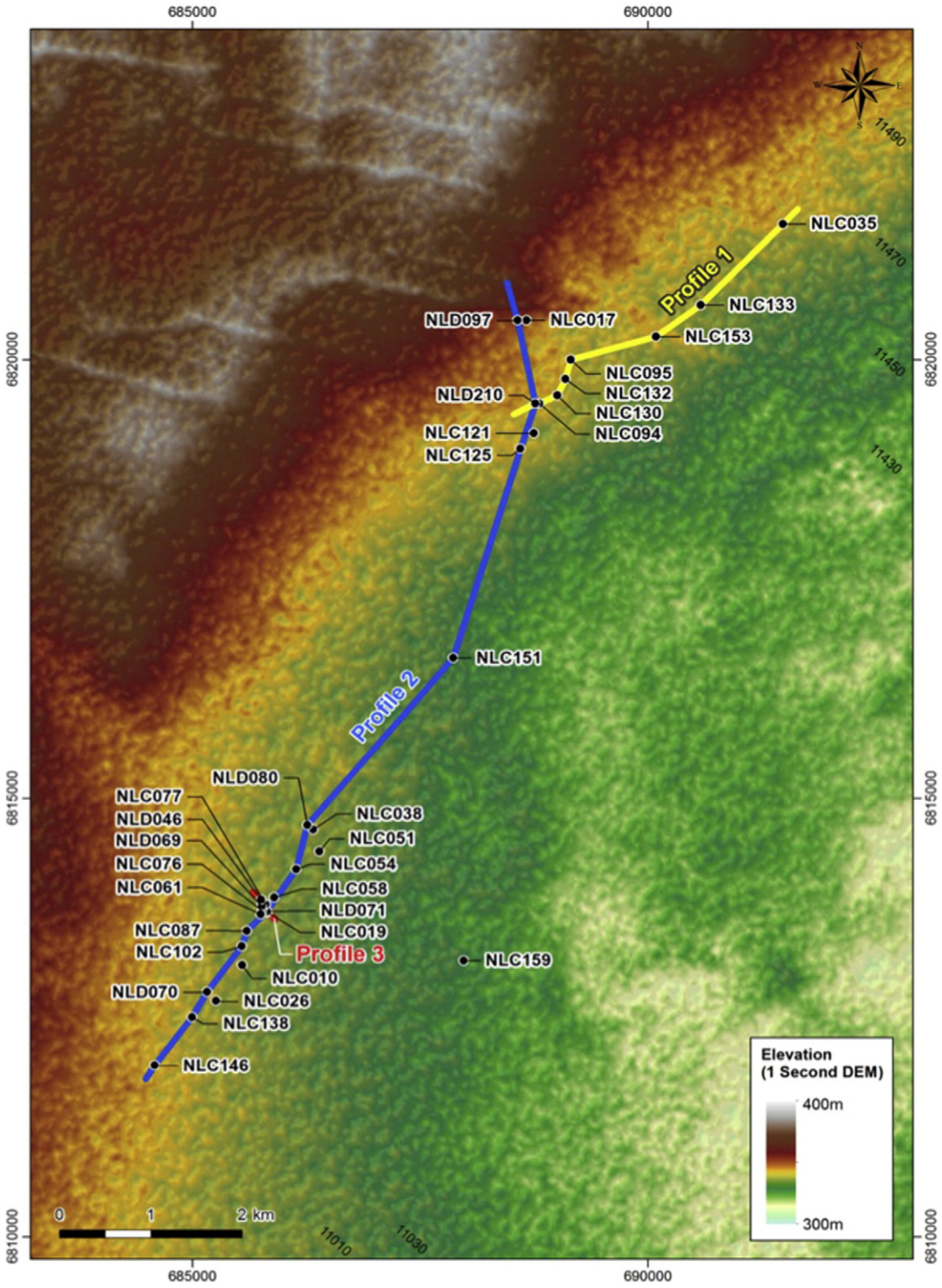

Fig. 9. Location of the reference conductivity-depth sections (profiles) for AEM validation via drill hole data. AEM Profiles 1 and 2 were designed to cross the northeast-southwest electrical conductivity gradient of the area, whereas AEM Profile 3 was designed to provide insights into the lateral variability of the regolith thickness.

permeable sedimentary units and crosscutting sedimentary packages. This is substantiated by the drill hole data in the area, in which sedimentary packages are widely present.

6.4. Regolith stratigraphy and mineralogy in the Neale study site: implications for AEM interpretation

Fig. 6 presents an idealized regolith stratigraphic sequence in the Neale site, and summarizes the stratigraphic and mineralogical framework of the cover. This stratigraphic sequence is the result of the direct logging of 32 drill holes. The thickness of the transported cover is between 2 and 25 m and is made of alluvial/colluvial dry ferruginous sands and gravels (90–98% quartz and ~10–1.5% kaolinite), which has a low electrical conductivity (e.g., This accords with the findings of Emerson and Yang, 1997; Emerson et al., 2000). This transported unit fits with the AEM interpretation of the less conductive unit at the top of the sections (Figs. 11 and 12). This unit corresponds primarily with unconsolidated sands at the surface, and with the ferruginous sands and gravels cemented with ferruginous cement at depth. These materials are poor electrical conductors and therefore appear resistive

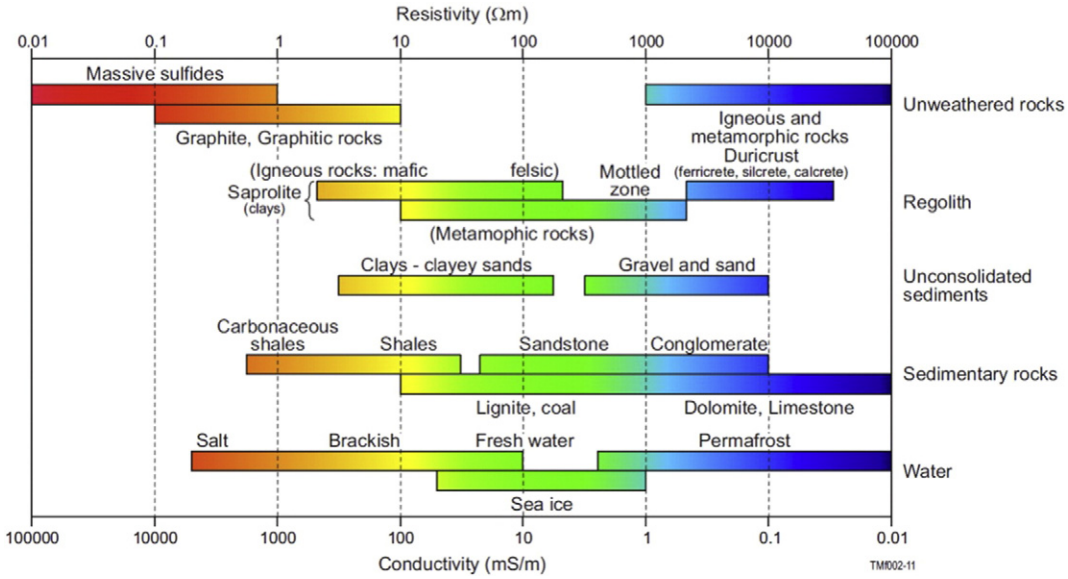

Fig. 10. Conductivity-resistivity values of various geological materials, spanning massive sulphides to graphite at high conductivities, to limestone, duricrust and silcrete with low conductivities (modified after Palacky, 1987). Clay and sand differ in conductivity by up to three orders of magnitude, similar to fresh versus saline water, respectively.

(blue) in the AEM interpreted conductivity-depth sections (e.g., Figs. 10, 11 and 12). Another factor that might influence observed EM response is that part of the regolith profiles are unsaturated and this masks the influence of groundwater conductivity response. Calcareous unit C is not displayed in the selected regolith profiles for Figs. 10, 11 and 12 since it is not present in those profiles.

The in situ regolith is divided into three units (following the key colour-letter legend from Fig. 11): (1) a laterally continuous silcrete unit (unit B; almost 100% quartz with traces of kaolinite); (2) an upper sandy, kaolinitic saprolite (unit D; ~50–75% quartz, 40–20% kaolinite); and (3) a lower ferruginous saprolite (unit E; ~25% quartz, 10–20% kaolinite, ~15% muscovite, 20–40% plagioclase + other minerals in minor abundance; Salama et al., 2016–in this issue).

The saprolitic package varies from 22 to 70 m in thickness. Unit B (silcrete) has a very low conductivity due to its lack of permeability (Enculescbu and Liescu, 1997), and therefore has a similar EM response as the transported cover in the EM conductivity-depth sections. The implication of a lack of conductivity contrast between the cover and the silicified upper in situ unit implies that the total thickness of the transported cover cannot be properly estimated. For this, drilling and field observations are essential. This accentuates the need for an integrated approach to the interpretation of AEM data, and how single technique interpretations may be misleading. In the regolith framework of the Neale area, electromagnetic interpretation without the consideration of the framework of the regolith profiles would have led to an error in the thickness determined for the transported cover of up to 20 m.

The upper saprolitic unit D is visible in the AEM profiles due to its conductivity contrast with the upper low conductives of the >90% quartz units in the transported cover-silcrete package, and the lower saprolite-fresh basement (made of more resistive minerals such as plagioclase and muscovite, with less porosity), whereas unit D is a mixture of sand/silt and kaolinite which enhances the conductivity response of this unit related to the units above and below, as well as due to an increase on porosity which would result in higher moisture and salts from groundwater. This contrast effectively delineates unit D in the interpreted AEM conductivity-depth sections (Figs. 11 and 12).

Figs. 11 and 12 display unit D from the drill logging, whereas in the EM profile signature, it shows a weak conductive response, which changes laterally. This apparent lateral change in conductivity could be interpreted as the result of lateral variability in mineralogy, textural features/moisture/salt content (e.g., Emerson and Yang, 1997; Munday et al., 2001). However, if the conductivity responses are interpreted together with the stratigraphic features of the regolith obtained directly by logging, unit D is a laterally continuous unit, although its mineral/textural and/or moisture/salt content may vary.

Previous studies on salinity of groundwater in regolith sequences related to different lithologies have reported that electrical conductivity response of the ground was dominated by the salinity of the groundwater or salt crystallized in the pore space of the regolith units (Emerson et al., 2000). The groundwater salinity of the Neale area is reported as 1000–3,000 mg/L TDS in Commander (1989); Fig. 1D). No direct bore hole data was available for sampling in this study.

It is important to notice that changes in the amount of kaolinite versus quartz in the absence of moisture may generate low conductivity changes and since the conductivity defined in the conductivity-depth sections (between ~100-500 mS/m) mineralogy and textural features may not account for this range alone, which suggests the influence of moisture and possible salts. The upper saprolite unit was sampled in serveral drill holes for whole-sample geochemical analysis and petrographic characterization in thin section. However, salts were not reported in any thin section, and a significant depletion in values of Na, Mg and Ca was described for all the samples reference to expected average values of Upper Continental Crust values (UCC; Rudnick and Gao, 2003; González-Álvarez et al., 2013). This seems to not support the presence of a significant amount of salts in the sampled upper saprolite unit. Based on these observations from field and geochemical data, we suggest that the changes in mineralogy proportions/texture/moisture/salts in unit D result in a more conductive response in the interpreted AEM conductivity-depth sections.

When this lateral apparent change in conductivity is integrated with an understanding of the vertical stratigraphic features of the regolith sequence, it was noted that in the drilling areas where unit D is more conductive, the silcrete unit above E is permeable. This permeability results in “windows”, which are more permeable to vertical fluid flow and therefore more prone to weathering than the silcrete duricrust observed in other drilling locations in the area.

To summarize: based on data integration (drill hole information, stratigraphy of the cover, mineralogy and geochemistry of the regolith units), the higher conductivity of unit D in specific areas is linked with a more intense vertical fluid mobility, resulting in changes in textural features, mineralogical proportions and/or moisture and salt content. This is stratigraphically associated with areas of more permeable silcrete at the top of the stratigraphic sequence.

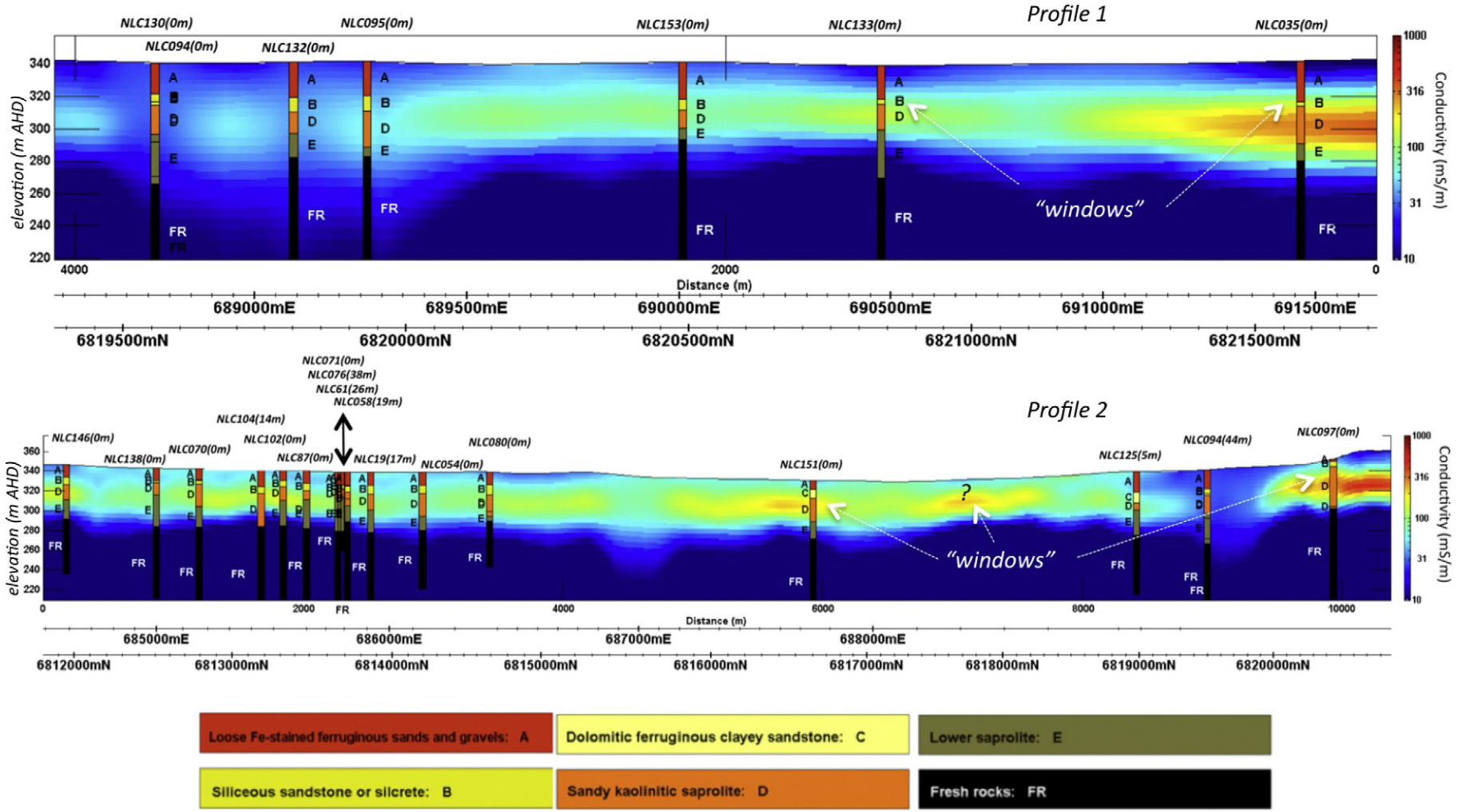

Fig. 11. AEM Conductivity-depth sections: Profile 1 and 2, which location is presented in Fig. 9. Two relatively high resistivity packages are present: (1) a surficial unit identified as unconsolidated sand/gravels and silcrete unit (A–B), and (2) unweathered basement rocks at depth (FR) are displayed as deep blue colour (10 mS/m). The most conductive zone (D; 70–300 mS/m, with most values between 100 and 200 mS/m) is associated with the upper saprolite unit in the in situ regolith stratigraphy, described from drill core. Notice that the most conductive segments of unit (D) coincide with a more permeable unit (B; silcrete) above.

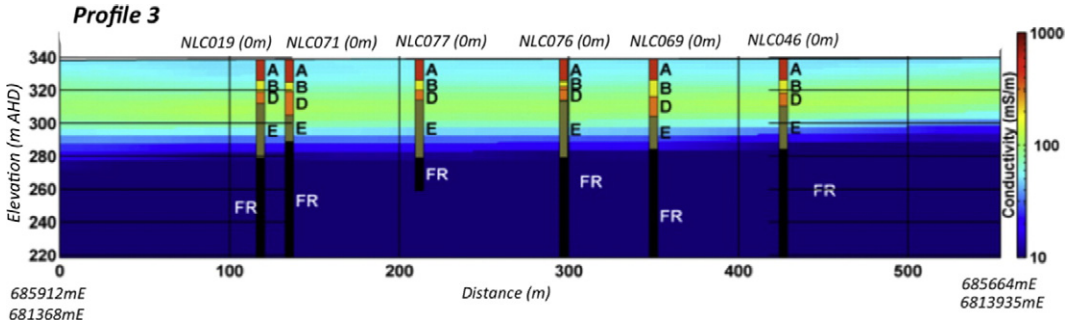

Fig. 12. AEM conductivity-depth section: Profile 3, which location is presented in Fig. 9. Six drill holes are located along the AEM flight line. This allows for a direct cross-reference between stratigraphic and mineralogical observations from the drill holes and the conductivity-depth sections are interpreted from AEM inversions. Overburden (A) and silcrete (B) are displayed in blue and light blue colour (20–50 mS/m) in the upper regolith profile, as well as in the upper (D) and lower (E) saprolite units. Unweathered rock is displayed in deep blue. Unit (C) is not displayed in this conductivity-depth section as it was not encountered during drilling. Colour legend as in Fig. 11.

The AEM data allowed the identification of these "windows" in other areas lacking direct drill hole observations (Fig. 11). In addition, AEM data was used to laterally link the conductivity of the stratigraphic units to the transported cover and the in situ regolith, allowing the inference of stratigraphic data between drill holes. This, combined with other geological datasets, allowed for the characterization of the regolith architecture for the Neale study site as dominated by flat and laterally continuous regolith units covering an irregular, undulating surface of the weathering front (basement surface).

This can have significant implications on the interpretation of exploration data. The areas above these silcrete "windows" are potentially the most reliable regions in which to obtain geochemical information from the basement rock units. Weathering of the basement rocks and hydromorphic dispersion processes through the regolith can reach the surface across these poorly cemented "windows". In other areas, where weathering profiles are protected by the silcrete unit, vertical fluid movement and element dispersion are likely occluded and hence do not reach the surface. Surface geochemical surveys should take this stratigraphic feature into consideration before they are designed, for a more efficient interpretation of the results.

6.5. Influence of the groundwater salinity on the AEM interpretation in the silver lake site

Grey (CSIRO unpublised datasets, personal communication, 2015) sampled water boreholes ~30 km east of the Silver Lake study site in the same palaeochannel structure (Figs. 1D and 8), reporting salinity values between 30,000 and >75,000 mg/L TDS for all boreholes sampled spanning from ~30 to ~100 km to the east. Commander (1989) reports similar values for the same palaeochannel (Fig. 1D). Company drilling made available for this research displayed large packages of transported cover with palaeochannel sand features with high porosity (Silver Lake Resources data).

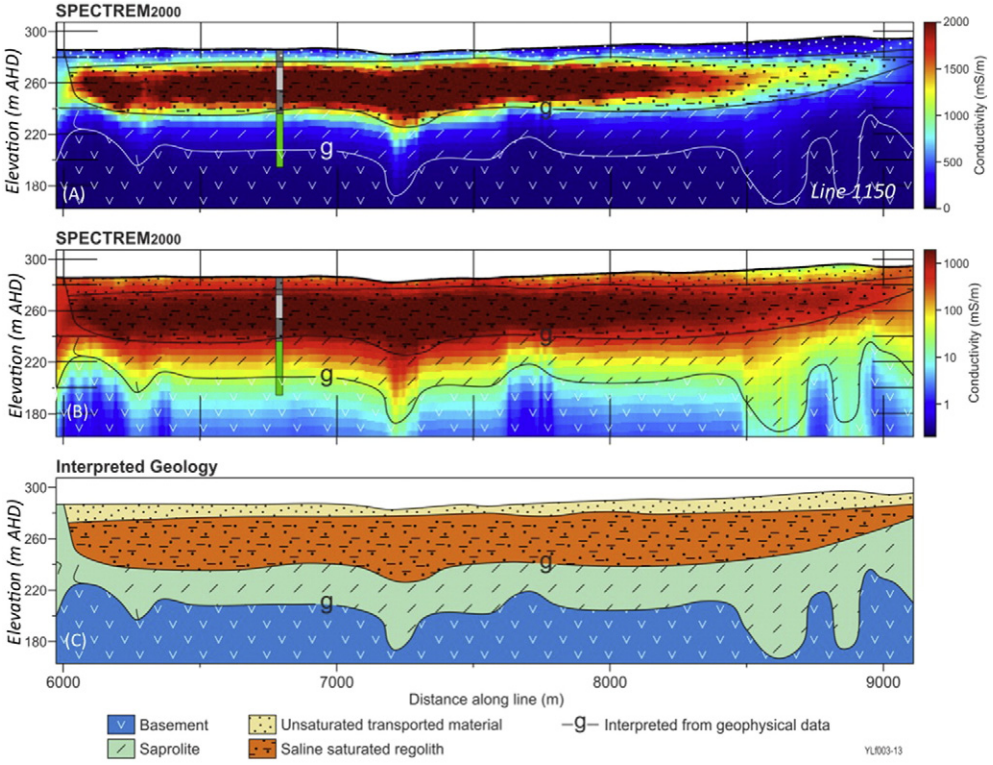

Fig. 13. Conductivity-depth section for line 1150 in Silver Lake (Fig. 3). Panels (A) and (B) display inverted $Spectrem_{2000}$ AEM data with a linear distribution of 0–2000 mS/m. The bottom panel (C) is the interpreted geological profile based on the inverted data. The AEM inverted models are ground truth with drill hole lithology. Total drill holes used for validation in the area were ~200, 4 for this line 1150. Drill hole colour code displays grey for overburden and green for basement rocks. The ~1500–2000 mS/m conductivity values, and the shape of the structure defined by the values are interpreted to define the geometry of the main palaeochannel in the Silver Lake study area saturated by hypersaline water.

In AEM interpretations, inaccurate prediction of shallow regolith areas may be due to the presence of saline water on the surface and within aquifers. Saline waters will attenuate most of the AEM signal, limiting its depth of exploration in these areas. The AEM response cannot capture enough conductivity contrast relating to regolith stratigraphy information within the cover to define regolith units or small scale features of the cover in such regions. However, in the Silver Lake area the boundary between the resistive basement and the overlying regolith was still able to be resolved, and the permeable sediment packages are well defined (Fig. 13).

In the Silver Lake area a projection of each bore hole logged with defined lithologies was performed on the nearest AEM line (Fig. 13). This was carried out in an effort to detect the correlation between drill logging and AEM conductive units. This work aimed at discriminating transported cover versus the in situ weathering profile, and attempted to differentiate the sedimentary units within sedimentary packages associated with the palaeochannel infills.

However, the total thickness of the sedimentary package was evident as the conductivity of the ground changes significantly when reaching basement rocks (Fig. 13). The geometry of the conductivity unit, flat at the top and concave at the bottom (Fig. 13), strongly suggests a palaeochannel sedimentary sequence associated with a more porous sedimentary unit saturated in saline water.

A detailed interpretation is presented in Fig. 13, which shows how inverted Line 1150 became a data-driven geological section. The interpreted profile has been cross-validated with drilling information (~200 drill holes were used to validate AEM conductivity-depth profiles in Silver Lake; four correspond to line 1150 in Fig. 13; one drill hole is displayed). This conductivity depth-slice describes vertically and laterally the geometry of a palaeochannel infill, highlighted by the conductivity of the saline water accumulated within the sedimentary package, since there is no variability on clay content, weathering features or porosity reported throughout the infill reported in the logging, petrography and XRD. This detailed geometric delineation is not traceable solely from surface remote sensing methods.

6.6. Geology and AEM data integration for trace element dispersion modelling and mineral exploration surface sampling

The geomorphological context where geochemical anomalies are detected is of key importance to understand their genesis (e.g., anomalies related to mechanical dispersion versus vertical chemical dispersion via fluids). The Neale tenement presents a low relief landscape with gentle slopes (Fig. 7). Within this geomorphological framework, the geochemical features observed in the transported cover are interpreted to be the result of erosion (lateral mechanical dispersion), and deposition of local basement rock suites and/or their weathering profiles associated with the erosion of breakaways. Therefore, the elements associated with these features appear to have been transported short distances (Figs. 1A and 7).

Metal anomalies, such as Au, have been described in previous studies from this area in transported cover under soil (González-Álvarez et al., 2013; Salama et al., 2016–in this issue). This Au could be displaced from its original source, but have originated nearby, most likely on the scale of hundreds of metres away in most cases. This could be traced by defining the associated transporting sedimentary system. Displaced Au anomalies may have originated from the northeast along the main geomorphological feature that possesses enough slope to be active for sedimentary processes (Figs. 1A and 7).

Saline water is concentrated in the riverine sedimentary sequences where porosity and permeability are high (e.g., Anand and Butt, 2010), and therefore can be used as a tracer in defining potential palaeovalleys and palaeochannels from groundwater salinity maps or AEM data (Fig. 1D). This salinity feature has significant effects on trace element mobility within the regolith and its expression at surface, since element dispersion is controlled mainly by fluid conditions: salinity, acidity (pH) and oxidation-reduction potential (Eh), with chemical ligands enhancing the mobility of many trace elements (e.g., Kerrich et al., 2002; González-Álvarez and Kerrich, 2010). In the Neale tenement, groundwater does not considerably increase the chemical trace element and metal mobility as much as other areas with hypersaline values of >30,000 mg/L TDS, reaching up to 290.000 mg/L TDS (Commander, 1989; Smyth and Barrett, 1994) associated with palaeochannels in the Yilgarn Craton (Fig. 1D).

However, surface geochemical sampling should not be discarded as a protocol in the Neale area to describe basement geochemical features, and should be conducted at different near surface depths to optimize the possibility of detecting geochemical features at depth in a regolith context.

As described previously, in the Neale tenement, the in situ regolith is divided into three units: (1) a laterally continuous silcrete unit (4–20 m thickness) with variations in the silica cement content; (2) a sandy, kaolinitic upper saprolite; and (3) a lower saprolite mainly expressed as ferruginous parental rock (granites, gneisses, schists and mafic rock suites). The upper and lower saprolite package varies from 18 to 50 m in thickness. The saprolite including the silcrete unit has a total thickness ranging from 22 to 70 m (Fig. 6).

Bulk chemical analyses throughout the regolith cover from previous studies (Salama et al., 2016–in this issue) indicate that in the regolith of Neale, SiO_2 decreases downwards from the surface unit (within 0–3 m), and is accompanied by a relative increase in Al_2O_3, TiO_2 and Fe_2O_3 contents. These oxides are the main chemical components of the Fe-stained kaolinite cement, as well as ferruginous pisoliths and nodules that form in the regolith units. Geochemically, the soil sample set is different from the deeper regolith units, featuring a Zr–Hf average content twice that of Upper Continental Crust (UCC) average values (Rudnick and Gao, 2003; Hu and Gao, 2008; González-Álvarez et al., 2013). This indicates that the aeolian soil cover is of recent exotic origin and therefore does not contain any significant geochemical link with the older, deeper, regolith units.

The location of key AEM conductivity-depth sections (Profiles 1, 2 and 3; Fig. 9), combined with drilling information, are interpreted to show a laterally continuous stratigraphic sequence with little variation across the landscape. However, as discussed in the previous section, the silcrete duricrust is not well developed in all locations, and a kaolinite-cemented grit or poorly-cemented sand is formed instead. The silcrete is most commonly seen as prominent duricrust protecting mesa landforms, and its lateral and subsurface extent is difficult to predict.

An impermeable silcrete unit capping the in situ regolith in the Neale tenement (Fig. 6) may have prevented the efficient vertical dispersion of trace elements to the surface. However, based on the combination of field and drilling observations, stratigraphy, mineralogy and AEM interpretation (Figs. 11 and 12) the lateral variation of the upper saprolite unit (D) in the sequence suggests the presence of permeable "windows" in the silcrete, which has been observed directly in areas with available drilling (Fig. 11). The surfaces above these "windows" are interpreted as the most reliable areas to obtain the best near-surface geochemical information derived from efficient vertical dispersion from the basement (Fig. 14). Further AEM interpretation may predict the location of other "windows" and assist in mapping a complete 3D architectural model of the cover.

7. Conclusions

Groundwater salinity in different regions has a significant influence on the observed AEM response and may hinder interpretation of the cover architecture. In low salinity groundwater areas AEM data may allow the lateral correlation of drilling data with high levels of confidence, thereby creating a 2D architectural model for the regolith cover, including its total thickness. However, since regolith thickness does not always correlate with sedimentary features, and can be the result of weathering fronts associated with shear corridors or fault structures, the total thickness variability should be carefully scrutinized.

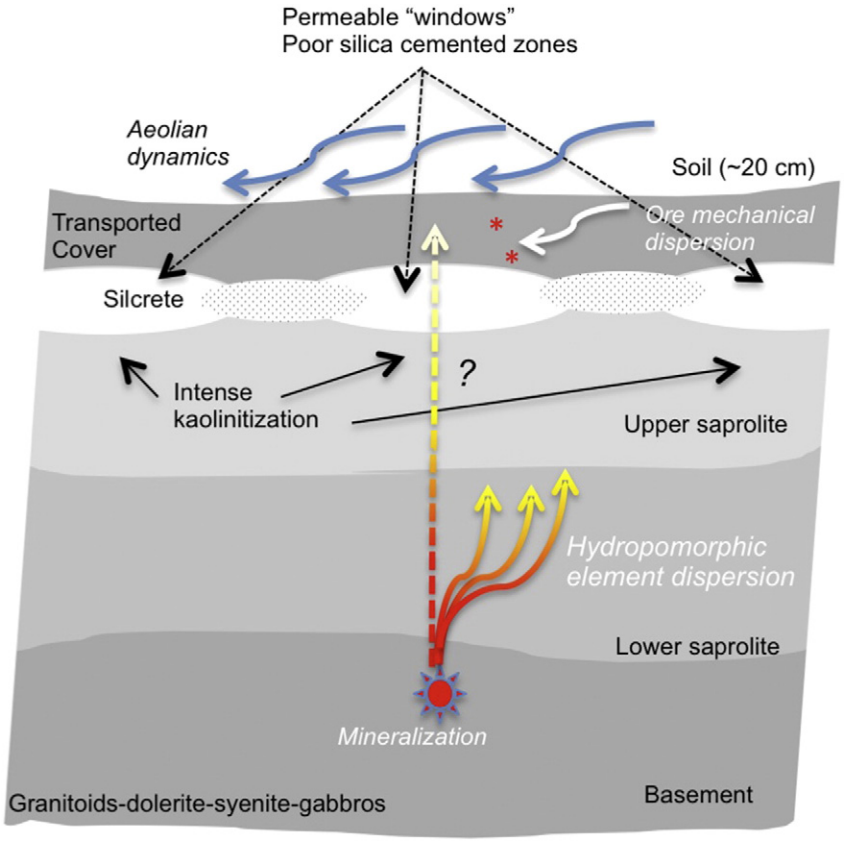

Fig. 14. Conceptual model for geochemical dispersion in the regolith for the Neale area. This model is the result of integrating drill hole observations, regolith stratigraphy and regolith mineralogy. AEM information allowed for lateral stratigraphic correlation, to enhance visualization of the overburden architecture. Based on this integration, the high porosity silcrete regions were highlighted, representing regions where AEM investigation may penetrate through the overburden to image the geology at depth. This model significantly assists in the design and interpretation of surface geochemical surveys in the area.

At the local scale (Neale study site), detailed interpretation of several datasets together with AEM data resulted in determination of the total regolith thickness (2 m–~65 m) and the thickness of a low conductive transported -silcrete package (~5–45 m) widely distributed in the area capping the upper saprolite. This latter package, via its conductivity contrast, upper saprolite sections can be associated to permeable areas of the silcrete unit ("windows"), interpreted as sections of more intense vertical fluid flow, and consequently a potentially higher vertical geochemical dispersion of the basement signature to the surface. AEM data allowed the prediction for the location of other possible "windows" where no direct drilling information was available. This can assist in building geochemical dispersion models, with direct implications on how to better interpret surface geochemical data in the area.

In the Silver Lake study site, with high electrical conductivity ground attributed to the presence of hypersaline groundwater. AEM data described a total regolith thickness of ~110 m, and data integration discovered the geometry of the main palaeochannel undercover in the area. This avoids the risk of drilling large thicknesses of cover when targeting fresh basement rocks.

Interpreted inverted AEM is much more than an approach to describe the electrical conductivity of the ground and detect positive conductors at depth as potential targets for mineral exploration. The availability of AEM data allows the lateral and vertical extension of the information contained in other geological datasets at specific locations. Therefore, when AEM data is interpreted and integrated in its geological context, it becomes a powerful tool to support mineral exploration in the Yilgarn Craton margin/Albany–Fraser Orogen region, having a significant impact to describe not only the cover architecture, but even improving geochemical dispersion models.

Acknowledgements

We would like to thank Beadell Resources Ltd. and Silver Lake Resources and Enterprise Connect for their funding contribution in the course of this research. Tania Ibrahimi is thanked for her professional help in drawing the maps and figures in this article. Ross Brodie and Geoscience Australia are specially acknowledged for his generosity sharing the use of the GA-LEI algorithm. Thank you to T. Prokopiuk, A. King and N. Reid for their comments in previous versions of this paper, and especially to two anonymous reviewers for their incisive review and insightful comments that have greatly improved this paper.

References

Anand, R.R., 2000. Regolith and geochemical synthesis of the Yandal Greenstone Belt. In: Phillips, G.N., Anand, R.R. (Eds.), Yandal Greenstone Belt, Regolith. Geology and Mineralisation. Australian Institute of Geoscientists Bulletin 31, pp. 79–112.

Anand, R.R., Butt, C.R.M., 2010. A guide for mineral exploration through the regolith in the Yilgarn Craton, Western Australia. Aust. J. Earth Sci. 57, 1015–1114.

Anand, R.R., Lintern, M., Noble, R., Aspandiar, M., Macfarlane, C., Hough, R., Stewart, A., Wakelin, S., Townley, B., Reid, N., 2014. Geochemical dispersion through transported cover in regolith-dominated terrains—toward an understanding of process. Soc. Econ. Geol. Spec. Publ. 18, 97–125.

Brodie, R.C., 2012. The Frome airborne electromagnetic survey, South Australia: implications for energy, minerals and regional geology. In: Roach, I.C. (Ed.), Appendix 3: GA-LEI Inversion of TEMPEST Data. Geoscience Australia Record 2012/40- DMITRE Report Book 2012/00003, pp. 278–287.

Butt, C.R.M., 1985. Granite weathering and silcrete formation on the Yilgarn Block, Western Australia. Aust. J. Earth Sci. 32, 415–432.

Butt, C.R.M., 2016. The development of regolith exploration geochemistry in the tropics and sub-tropics. Ore Geol. Rev. 73, 380–393 (2016–in this issue, Special Issue).

Butt, C.R.M., Lintern, M.J., Anand, R.R., 2000. Evolution of regoliths and landscapes in deeply weathered terrain — implications for geochemical exploration. Ore Geol. Rev. 16, 167–183.

Cassidy, K.F., Champion, D.C., Krapež, B., Barley, M.E., Brown, S.J.A., Blewett, R.S., Groenewald, P.B., Tyler, I.M., 2006. A revised geological framework for the Yilgarn Craton, Western Australia. Western Australia Geological Survey, Record 2006/8.
Christiansen, A.V., Auken, E., 2010. A Global Measure for Depth of Investigation in EM and DC Modelling: ASEG Extended Abstracts, 1–4.
Clark, D.J., 2009. Palaeovalley, palaeodrainage, and palaeochannel — what's the difference and why this matters? Trans. R. Soc. S. Aust. 133, 57–61.
Commander, D.P., 1989. Western Australia Groundwater Salinity Map, Scale (1:10,000,000). Geological Survey of Western Australia, Australia.
Davies, A., 2013. 6th International Conference in Airborne Electromagnetics (AEM 2013). Exploration Geophysics Special Issue vol. 46 (1) (139 pp.).
De Broekert, P., 2002. Origin of Tertiary inset-valleys and their fills, Kalgoorlie, Western Australia. PhD Thesis, Australian National University, Canberra, (unpublished), 388 pp.
De Broekert, P., Sandiford, M., 2005. Buried inset-valleys in the eastern yilgarn craton, Western Australia: geomorphology, age, and allogenic control. J. Geol. 113, 471–493.
Doyle, M.G., Fletcher, R.I., Foster, J., Large, R.R., Mathur, R., McNaughton, N.J., Meffre, S., Muhling, J.M., Phillips, D., Rasmussen, B., 2015. Geochronological constraints on the Tropicana gold deposit and Albany–Fraser orogen, Western Australia. Society of economic geologists, Inc. Econ. Geol. 110, 355–386.
Emerson, D.W., Yang, Y.P., 1997. Effects of water salinity and saturation on the electrical resistivity of clays. Preview 68, 19–24.
Emerson, D.W., Macnae, J., Sattel, D., 2000. Physical properties of the regolith in the Lawler's area, Western Australia. Explor. Geophys. 31, 229–235.
Enculescbu, I., Liescu, I., 1997. Electrical conductivity of quartz crystals. Cryst. Res. Technol. 32, 879–891.
Fitterman, D.V., Stewart, M.T., 1986. Transient electromagnetic sounding for groundwater. Geophysics 51, 995–1005.
Gallant, J.C., Dowling, T.I., 2003. A multi-resolution index of valley bottom flatness for mapping depositional areas. Water Resour. Res. 39, 1347 (4–1/4–13).
González-Álvarez, I., Kerrich, R., 2010. REE and HFSE mobility due to protracted flow of basinal brines in the Mesoproterozoic Belt-Purcell Supergroup, Laurentia. Precambrian Res. 177, 291–307.
González-Álvarez, I., Salama, W., Anand, R.R., Sweetapple, M., Abdat, T., leGras, M., Hough, R., Walshe, J., 2013. Trace element mobility in a deeply weathered cover profile in the Albany–Fraser Orogen/Yilgarn Craton Margin: the Hercules and Atlantis gold prospects. Internal CSIRO Technical Report, EP1310336, 81 pp + digital appendices.
González-Álvarez, I., Boni, M., Anand, R.R., 2015a. Mineral exploration in regolith-dominated terrains: global considerations and challenges. Ore Geol. Rev. (Special Issue, in this issue-a).
González-Álvarez, I., Salama, W., Anand, R.R., 2016. Sea-level changes and buried islands in a complex coastal palaeolandscape in the South of Western Australia: Implications for greenfield mineral exploration. Ore Geol. Rev. 73, 475–499 (Special Issue, in this issue).
Gray, J.D., 2001. Hydrogeochemistry in the Yilgarn Craton. Geochem. Explor. Environ. Anal. 1, 253–264.
Hu, Z., Gao, S., 2008. Upper crustal abundances of trace elements: a revision and update. Chem. Geol. 253, 205–221.
Kerrich, R., Renaut, R.W., Bonli, T., 2002. Trace-element composition of cherts from alkaline lakes in the east African rift: a probe for ancient counterparts. In: Renaut, R.W., Ashley, G.M. (Eds.), Sedimentation in Continental Rifts. Soc. Sed. Geol., Boulder, CO, pp. 277–298 (Spec. Publ. 73).
Kirkland, C.L., Spaggiari, C., Smithies, R.H., Wingate, M.T.D., Belousova, E.A., Gréau, Y., Sweetapple, M.T., Watkins, R., Tessalina, S., Creaser, R., 2015. The affinity of Archean crust on the Yilgarn—Albany–Fraser Orogen boundary: implications for gold mineralisation in the Tropicana Zone. Precambrian Res. 266, 260–281.
Kyser, K., Hiatt, E., Renac, C., Durocher, K., Holk, G., Deckart, K., 2000. Diagenetic fluids in paleo- and mesoproterozoic sedimentary basins and their implications for long protected fluid histories. In: Kyser, K. (Ed.), Fluids and Basin EvolutionMineral Association of Canada 28. Short Course Series, Kingston, Ontario, pp. 225–262.
Leggatt, P.B., Klinkert, P.S., Hage, T.B., 2000. The spectrem airborne electromagnetic system—further developments. Geophysics 65, 1976–1982.
Ley Cooper, A.Y., 2013. Airborne EM in the Albany–Fraser. Internal CSIRO report, EP131015 (69 pp.).
Ley-Cooper, A.Y., Brodie, R., 2013. Inversion of spectrem AEM data for conductivity and system geometry. 23rd International Geophysical Conference and Exhibition in Melbourne, Australia, August 2013, Conference Proceedings vol. 1, pp. 1–4. http://dx.doi.org/10.1071/ASEG2013ab145.
Ley-Cooper, A.Y., González-Álvarez, I., 2014. Full inversion of AEM data to assist exploration strategies in a regolith dominated terrain: Yilgarn Craton, Western Australia. The 13th SAGA Biennial Conference, South Africa, October 2013, Conference Proceedings Volume, pp. 145–146.
Ley-Cooper, A.Y., Munday, T.J., 2013. Groundwater assessment and aquifer characterization in the Musgrave Province South Australia: interpretation of SPECTREM airborne electromagnetic data. Goyder Institute for Water Research, Technical Report Series 13/7.
Ley-Cooper, Y., Macnae, J., Tweed, S., 2008. Estimating subsurface porosity and salt loads using airborne geophysical data. Near Surf. Geophys. 6, 31–37.
Lintern, M.J., 2015. The association of gold with calcrete. Ore Geol. Rev. 66, 132–199.
Macnae, J., Smith, R., Polzer, B.D., Lamontagne, Y., Klinkert, P.S., 1991. Conductivity depth imaging of airborne electromagnetic step response data. Geophysics 56, 102–114.
Munday, T., 2009. Regolith Geophysics. In: Scott, K., Pain, C. (Eds.), Regolith Science. CSIRO Publishing, Australia, pp. 219–247.
Munday, T.J., Macnae, J., Bishop, J., Sattel, D., 2001. A geological interpretation of observed electrical structures in the regolith: lawlers, Western Australia. Explor. Geophys. 32, 36–47.
Munday, T., Fitzpatrick, A., Reid, J., Berens, V., Sattel, D., 2007. Frequency and/or Time Domain HEM Systems for Defining Floodplain Processes Linked to the Salinisation Along the Murray River? ASEG 2007-Perth. Western Australia (5 pp.).
Nesbitt, H.W., Young, G.M., 1982. Early Proterozoic climates and plate motions inferred from major element chemistry of lutites. Nature 299, 715–717.
Pare, P., Gribenko, A.V., Cox, L.H., Čuma, M., Wilson, G.A., Zhdanov, M.S., Legault, J., Smit, J., Polome, L., 2012. 3D inversion of SPECTREM and ZTEM airborne electromagnetic data from the Pebble Cu–Au–Mo porphyry deposit. Alaska. Explor. Geophys. 43 (2), 104–115.
Palacky, G.V., 1987. Resistivity characteristics of geologic targets. Electromagnetic Methods in Applied Geophysics, SEG 1351.
Palacky, G.J., Ritsema, I.L., de Jong, 1981. Electromagnetic prospecting for groundwater in Precambrian terrains in the Republic of Upper Volta. Geophys. Prospect. 29, 932–955.
Pillans, B., 2005. Geochronology of the Australian Regolith. In: Anand, R.R., De Broekert, P.P. (Eds.), Regolith Landscape Evolution Across Australia. CRC LEME, Australia.
Porto, C.G., 2016. Geochemical exploration challenges in the regolith dominated Igarapé Bahia gold deposit, Carajás, Brazil. Ore Geol Rev. 73, 432–450 (Special Issue, in this issue).
Reid, J.E., Munday, T., Fitzpatrick, A., 2007. High-resolution airborne electromagnetic surveying for dry land salinity management: the Toolibin Lake SkyTEM case study. ASEG 2007-Perth. Australia, Western (5 pp.).
Robertson, I.D.M., 1996. Ferruginous lag geochemistry on the Yilgarn Craton of Western Australia; practical aspects and limitations. J. Geochem. Explor. 57, 139–151.
Rudnick, R.L., Gao, S., Rudnick, R.L., Holland, H.D., Turekian, K.K., 2003. The composition of the continental crust. The CrustTreatise on Geochemistry vol. 3. Elsevier, Oxford, New York, pp. 1–64.
Rutherford, J., Munday, T., Meyers, J., Cooper, M., 2001. Relationship between regolith materials, petrophysical properties, hydrologeology and mineralization at the Cawse Ni laterite deposits, Western Australia: implications for exploring with airborne EM. Explor. Geophys. 32, 160–170.
Salama, W., González-Álvarez, I., Anand, R.R., 2016. Significance of weathering and regolith/landscape evolution for mineral exploration in the NE Albany-Fraser Orogen, Western Australia. Ore Geol. Rev. 73, 500–521 (Special Issue, in this issue).
Smith, R.E., 1983. Geochemical exploration in deeply weathered terrain. Discussion papers of the CSIRO Division of Mineralogy, Short Course, March 1983, Perth, Western Australia, pp. 109–154.
Smith, R.E., Perdrix, J.L., Davis, J.M., 1987. Dispersion into pisolitic laterite from the greenbushes mineralized Sn-Ta pegmatite system, Western Australia. J. Geochem. Explor. 28, 251–265.
Smith, R.E., Birrell, R.D., Brigden, J.F., 1989. The implications to exploration of chalcophile corridors in the Archaean Yilgarn Block, Western Australia, as revealed by laterite geochemistry. J. Geochem. Explor. 32, 169–184.
Smyth, E.L., Barrett, D.M., 1994. Geophysical characteristics of the tertiary palaeochannels in the Yilgarn block, Western Australia. Geophysical Signatures of Western Australian Mineral Deposits. Geology and Geophysics Department & UWA Extension, The University of Western Australia, Publication 26, pp. 417–425.
Spaggiari, C.V., Kirkland, C.L., Smithies, R.H., Wingate, M.T.D., Belousova, E.A., 2015. Transformation of an Archaean Craton margin during Proterozoic basin formation and magmatism: the Albany–Fraser orogen, Western Australia. Precambrian Res. 266, 440–466.
Spies, B.R., Fitterman, D., Holladay, S., Liu, G., 1998. Airborne electromagnetics. Explor. Geophys. 29.
Vearncombe, J.R., Kohler, E., Meyers, J., Phillips, N., Rothery, E., Ryan, D., 2000. Regional, structural and exploration geology in a terrain with minimal outcrop — the yandal belt. AIG Bull. 32, 17–39.
Worrall, L., Munday, T.J., Green, A.A., 1999. Airborne electromagnetics — providing new perspectives on geomorphic process and landscape development in regolith-dominated terrains. Phys. Chem. Earth (A) 24, 855–860.
Worrall, L., Lane, R., Meyers, J., Whitaker, A., 2001. Exploring through cover — the integrated interpretation of high resolution aeromagnetic, airborne electromagnetic and ground gravity data from the grant's patch area, Eastern Goldfields Province, Archaean Yilgarn Craton Part A: mapping geology using airborne electromagnetics (TEMPEST). Explor. Geophys. 32, 190–193.
Xueqiu, W., Bimin, Z., Xin, L., Shanfa, X., Wensheng, Y., Rong, Y., 2016. Geochemical challenges of diverse regolith-covered terrains for mineral exploration in China. Ore Geol. Rev. 73, 417–431 (in this issue).